Politecnico di Milano

POLITECNICO
MILANO 1863

Final Report Functional Mechanical Design - Group 4

Design of a Mechanism of an Automatic Machine for Soap Production

Alberto Giammarino
Andrea Caloni
Paolo Fasoli
Gregory Helfrich
Mahmoud Aly

Hand-in date: 29th October 2020
Tutors: Simone Cinquemani, Daniele Catelani and Francesco Bono

Contents

List of Figures iii

List of Tables v

1 Problem Statement 1

2 Motion Law Design 5
- 2.1 Introduction . . . 5
- 2.2 Design First Motion Law . . . 5
  - 2.2.1 Motion Law choice . . . 6
  - 2.2.2 Design Procedure Modified Trapezoidal Law . . . 7
  - 2.2.3 Motion Law Obtained . . . 7
- 2.3 Design Second Motion Law . . . 11

3 Cams Synthesis 15
- 3.1 Synthesis First Cam . . . 15
- 3.2 Synthesis Second Cam . . . 17
  - 3.2.1 Design Parameters . . . 17
  - 3.2.2 Influence of β_0 and l on Cam Design . . . 18
  - 3.2.3 Design Parameters Choice . . . 20

4 Adams Model and Simulation Analysis 22
- 4.1 Introduction . . . 22
- 4.2 Model Description . . . 22
- 4.3 Kinematic Analysis . . . 24
- 4.4 Dynamic Analysis . . . 26
  - 4.4.1 Real contacts . . . 26
  - 4.4.2 Motor Torque . . . 26
  - 4.4.3 First Dynamic Analysis . . . 27
  - 4.4.4 Second Dynamic Analysis . . . 29

5 Motor Sizing 40
- 5.1 Requirements . . . 40
- 5.2 Choice of Transmission and Motor . . . 41

6 Alternative Design 43
- 6.1 Possible Alternative Solutions . . . 43
- 6.2 Dynamic Analysis using Alternative Design . . . 43
  - 6.2.1 Motion Law Comparison . . . 43
  - 6.2.2 Contact Forces Comparison . . . 45

6.2.3 Slippage Check 46
6.2.4 Motor Torque Comparison 48

Bibliography **50**

List of Figures

1.1 Automatic Machine with the main subsystems: 1. Press, 2. Upload of raw material, 3. Turning pad, 4. Discharge of products 1
1.2 Uploading Subsystem 2

2.1 Geometrical Acceleration of the Modified Trapezoidal Motion Law. α_s is the total rise angle. 6
2.2 Adimensional Position First Motion Law 8
2.3 Adimensional Velocity First Motion Law 8
2.4 Adimensional Acceleration First Motion Law 9
2.5 Adimensional Jerk First Motion Law 9
2.6 Adimensional V*A First Motion Law 10
2.7 Left: c_v and c_a dependency on d_1; Right: c_k dependency on d_1. 12
2.8 Dependency of Maximum Jerk on d_1 12
2.9 Left: pressure angle trend of Second Cam with $d_1 = 0.1$; Right: pressure angle trend of Second Cam with $d_1 = 0.4$. 13

3.1 First Cam Profiles 16
3.2 Pressure Angle First cam 16
3.3 Parameters for Second Cam Synthesis 17
3.4 Example trend Pressure Angle Second Cam 18
3.5 Initial Pressure Angle of Second Cam as function of β_0 and l 19
3.6 Final Pressure Angle of Second Cam as function of β_0 and l. The circles correspond to the minimum of each curve. 19
3.7 Second Cam Profile 20

4.1 MSC Adams Model 23
4.2 Comparison between designed motion law and motion law obtained from kinematic analysis using MSC Adams for the first follower 24
4.3 Comparison between designed motion law and motion law obtained from kinematic analysis using MSC Adams for the second follower 24
4.4 Feed-Forward Torque 25
4.5 Contact Parameters 26
4.6 Dynamic Analysis Motion Laws Slider 27
4.7 Dynamic Analysis Motion Laws Second Follower 27
4.8 External and Internal Contact First Cam 28
4.9 Contact Second Cam 28
4.10 Torsion Spring Catalogue, LeeSpring 29
4.11 Dynamic Analysis Motion Laws Slider with Torsional Spring 30
4.12 Dynamic Analysis Motion Laws Second Follower with Torsional Spring . . . 30
4.13 External and Internal Contact First Cam with Torsional Spring 31

4.14 Contact Second Cam with Torsional Spring 31
4.15 Phase 1 Simulation 32
4.16 Phase 2 Simulation 32
4.17 Phase 3 Simulation 33
4.18 Phase 4 Simulation 33
4.19 Phase 5 Simulation 34
4.20 Slipping Check Internal Contact First Cam 34
4.21 Slipping Check External Contact First Cam 35
4.22 Slipping Check Contact Second Cam 35
4.23 Contact Pressure Internal Profile First Cam 36
4.24 Contact Pressure External Profile First Cam 37
4.25 Contact Pressure Second Cam 37
4.26 Cam Contact Hertz Stress as Function of Cam Hardness and Material Type 38

5.1 Torque demanded by the system 40
5.2 Miksan Motor Catalogue 41

6.1 Comparison First Motion Law: left alternative design, right previous design 44
6.2 Comparison Second Motion Law: left alternative design, right previous design 44
6.3 Comparison Contact Force First Cam: left alternative design, right previous design 45
6.4 Comparison Contact Force Second Cam: left alternative design, right previous design 45
6.5 Slipping Check Internal Contact First Cam Alternative Design 46
6.6 Slipping Check External Contact First Cam Alternative Design 46
6.7 Slipping Check Contact Second Cam Alternative Design 47
6.8 Comparison Motor Torque: left alternative design, right previous design . . 48

List of Tables

1.1 Motion Law Specifications 2

2.1 Motion Law Specifications x 5
2.2 Performance Parameters First Motion Law 7
2.3 Motion Law Specifications θ 11
2.4 Performance Parameters First Motion Law 11

3.1 Design Parameters First Cam 16
3.2 Design Parameters Second Cam 20

5.1 Load parameters 40
5.2 Parameters Motor Chosen 41

6.1 Load parameters using Alternative Design 48

1 Problem Statement

The current project is about the design of a mechanism of an Automatic Machine for soap production. The automatic machine considered is depicted in figure 1.1. It is composed of four functional groups carrying out the following operations:

1. Production of the desired soap shapes out of the raw material using a press.
2. Taking the incoming raw soap and uploading it on a turning pad.
3. Sustaining the raw soap during operation while easing its charge and discharge.
4. Discharging the obtained soap shapes.

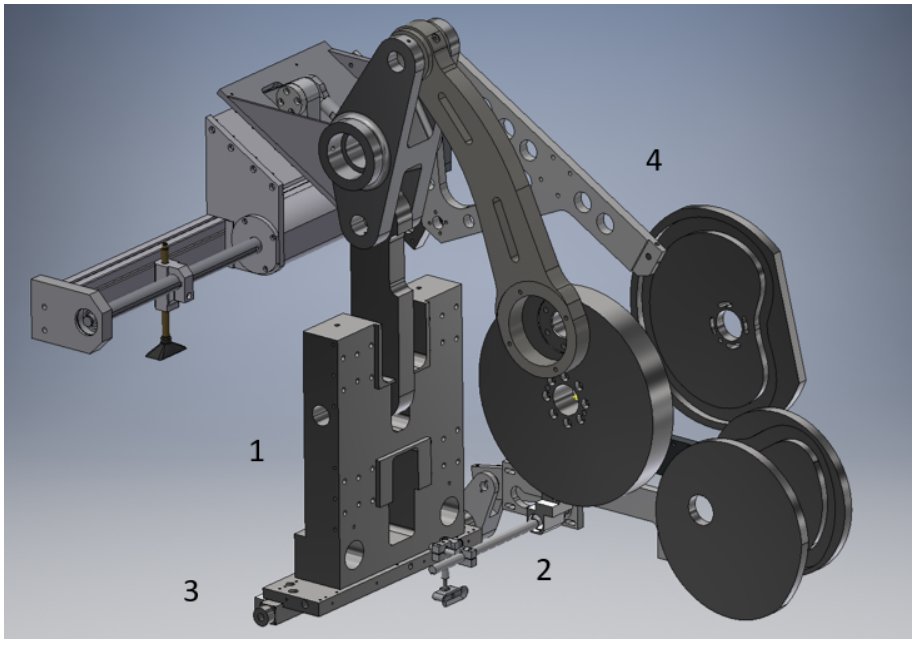

Figure 1.1: Automatic Machine with the main subsystems: 1. Press, 2. Upload of raw material, 3. Turning pad, 4. Discharge of products

The purpose of the project is to design one of the first three subsystems described above. In this report the design of the second functional group is discussed. The final mechanism to be designed is shown in figure 1.2. This apparatus implements movements that allow the uploading arm to move the raw soap material that has entered the system to the turning pad, where it is then shaped and removed from the machine. This movement can be obtained by combining the linear movement x to the angular movement θ.

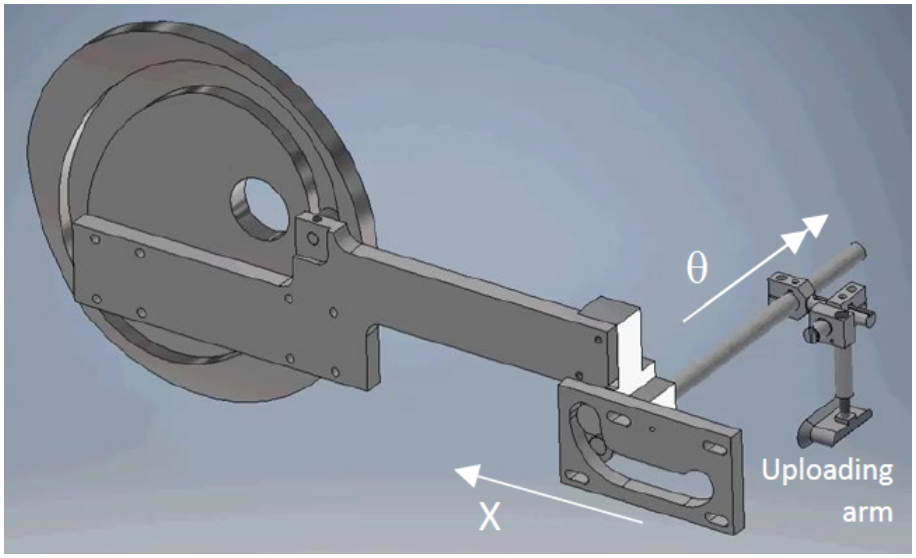

Figure 1.2: Uploading Subsystem

The following data was given:

- Mass of the slider $m_1 = 4.5kg$.
- Mass and momentum of inertia with respect to the axis of rotation of the moving arm $m_2 = 1.2kg$ and $J = 0.5kgm^2$, respectively.
- Motion law specifications reported in table 1.1, where α is the master angle, x is the linear displacement of the slider and θ is the angular displacement of the uploading arm.
- Rotational speed of the master shaft at steady-state, which is $180°/s$.

α[°]	x [mm]	θ[°]
0	0	0
100	160	0
130	180	90
170	180	90
200	160	0
360	0	0

Table 1.1: Motion Law Specifications

Considering that the driving element moves with a constant angular speed, it is necessary to:

1. Design the motion law of the moving arm along the two directions;
2. Synthesize the two cam mechanisms

3. Analyze the mechanism through kinematic parameters (pressure angles and undercut) and compute the motion law obtained with the designed mechanism
4. Calculate forces transmitted and the motor torque with a multibody model.
5. Critically evaluate the feasibility of the system

2 Motion Law Design

2.1 Introduction

The system under analysis requires the design of two motion laws, one for the translation of the slider and one for the rotation around the rotational axis of the uploading arm. The following preliminary choices have been made for the design of the two motion laws:

1. Rise and fall of the two motion laws should be symmetric so that the roller center of the second follower always travels the same path when moving back and forth.
2. The slider should not stop at the point $\alpha = 100°$ $x = 160mm$ because this would create a sudden change in direction of the trajectory of the second cam resulting in higher complexity and eventually impossibility in generating the desired motion.
3. Only motion laws guaranteeing the continuity of the acceleration are used in order to avoid as much undesired vibrations of the system as possible.

2.2 Design First Motion Law

In table 2.1 the slider motion law specifications are reported along with the phase which starts at the specific point. Notice that an additional point is present with respect to table 1.1 since the final 60° of cam rotation are not exploited for enlarging the fall phase in order to keep the rise and fall symmetric. Thus, only the design of the rise phase is discussed in this section.

$\alpha[°]$	x [mm]	Phase
0	0	Rise
100	160	”
130	180	Dwell
170	180	Fall
200	160	”
300	0	Dwell
360	0	

Table 2.1: Motion Law Specifications x

2.2.1 Motion Law choice

As previously mentioned, all the motion laws having discontinuities in the acceleration are discarded. Thus, the laws which can be used are:

1. Cycloidal law.
2. Trapezoidal laws.
3. Modified trapezoidal laws.

Since more degrees of freedom are needed to enforce the crossing of an intermediate point, the cycloidal law is discarded. The difference between trapezoidal laws and modified trapezoidal laws is that the latter are obtained from the former by smoothing the edges of the acceleration law using sinusoidal segments. As stated in [1], modified trapezoidal laws have smaller accelerations but higher jerk than trapezoidal laws given the same ratio t_0/t_s, where t_0 is the time length of the segment used to avoid acceleration discontinuity and t_s is the total rise time. Since it is preferred to keep the maximum acceleration small and it is considered enough to avoid infinite values of jerk, the modified trapezoidal law, which general shape is shown in figure 2.1, is chosen for the design.

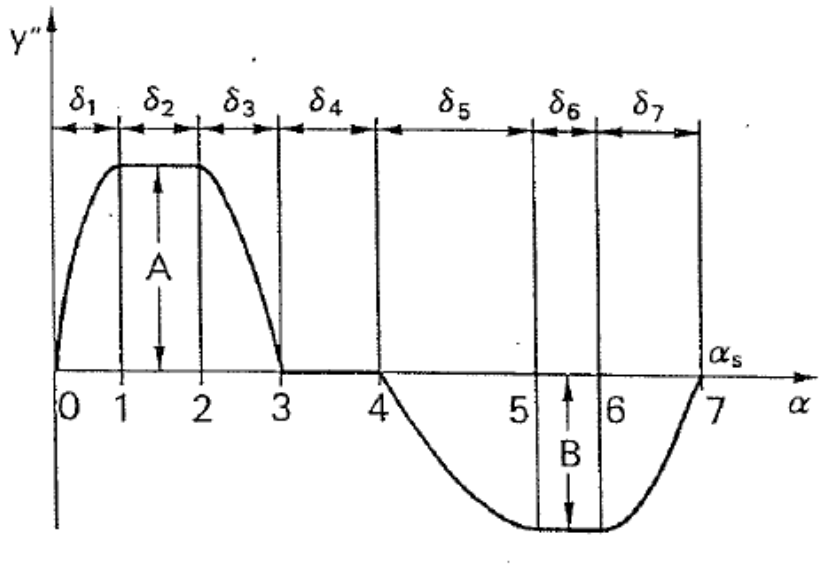

Figure 2.1: Geometrical Acceleration of the Modified Trapezoidal Motion Law. α_s is the total rise angle.

2.2.2 Design Procedure Modified Trapezoidal Law

For the sake of clarity, a generic point P is defined as $P = (\alpha[^\circ], x[mm])$. Referring to figure 2.1, it is desired that the slider starts and finishes with zero speed and goes from $0 = (0, 0)$ to $7 = (130, 180)$ passing through $(100, 160)$. Thus, the boundary and intermediate conditions are parametrized as a function of the constants of integration, A, B and two of the seven δs. Many formulations of this problem are possible; it is chosen that $5 = (100, 160)$ and the system of equations 2.2 is solved in order to find the constants of integration, A, B, δ_6 and δ_7, while the other δs are free but chosen to ensure that equation 2.1 is fulfilled.

$$\sum_{i=1}^{7} \delta_i = \alpha_s \tag{2.1}$$

$$\begin{cases} y_0 = 0 \\ y_0^{'} = 0 \\ y_7 = 180 \\ y_7^{'} = 0 \\ y_5 = 160 \\ \delta_6 + \delta_7 = \alpha_r \end{cases} \tag{2.2}$$

where $\alpha_r = 30^\circ$ is the remaining master angle when point 5 is reached.

2.2.3 Motion Law Obtained

After having performed some studies on how the main performance parameters vary depending on the initial choice of the free δs, a motion law has been selected, having fractions of the rise angle:

$$\frac{\delta}{\alpha_s} = \begin{bmatrix} 0.2 & 0.1 & 0.25 & 0.0 & 0.2192 & 0.1393 & 0.0915 \end{bmatrix}$$

The performance parameters obtained are reported in table 2.2 and the resulting plots of the adimensional law obtained are depicted from figure 2.2 to figure 2.6.

c_v	c_a^+	c_a^-	c_k
1.89	5.62	4.91	7.36

Table 2.2: Performance Parameters First Motion Law

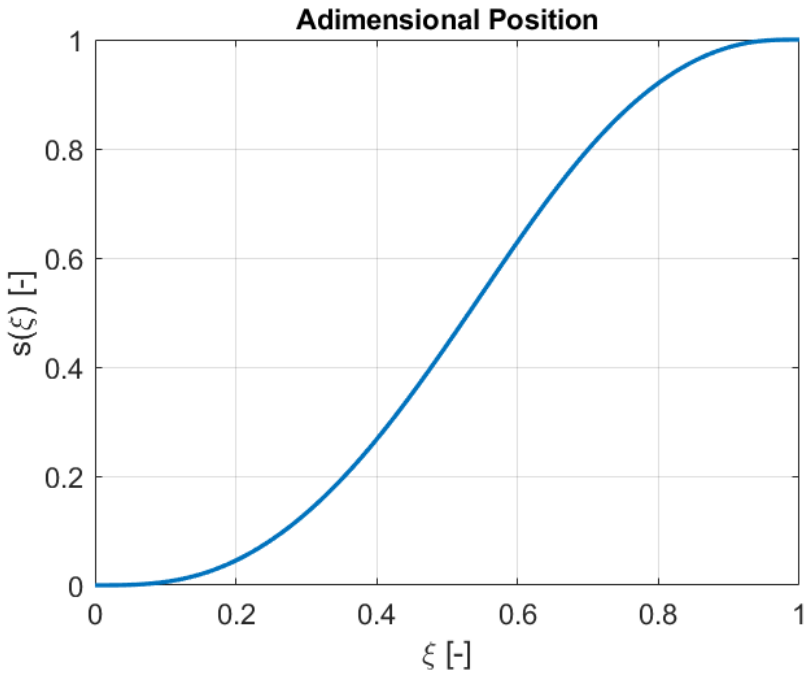

Figure 2.2: Adimensional Position First Motion Law

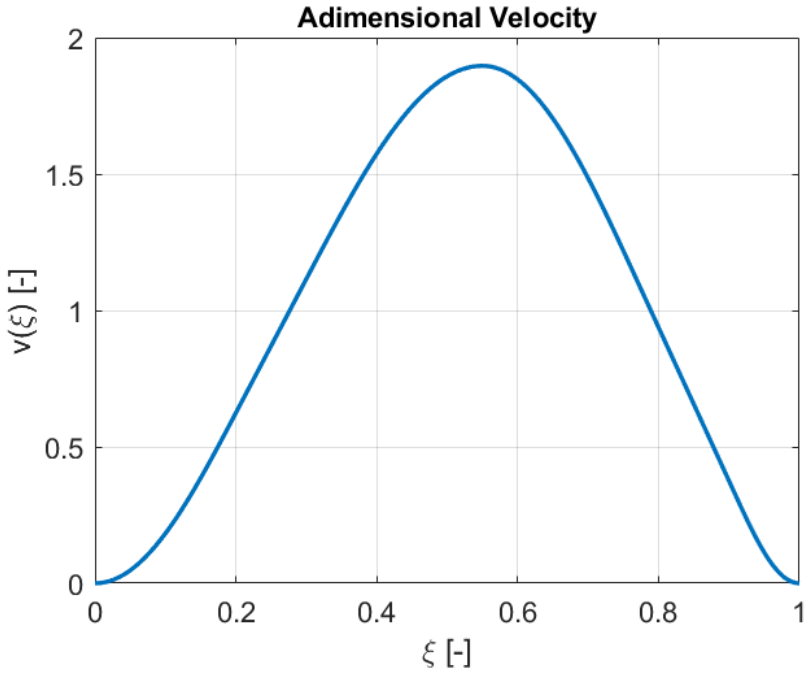

Figure 2.3: Adimensional Velocity First Motion Law

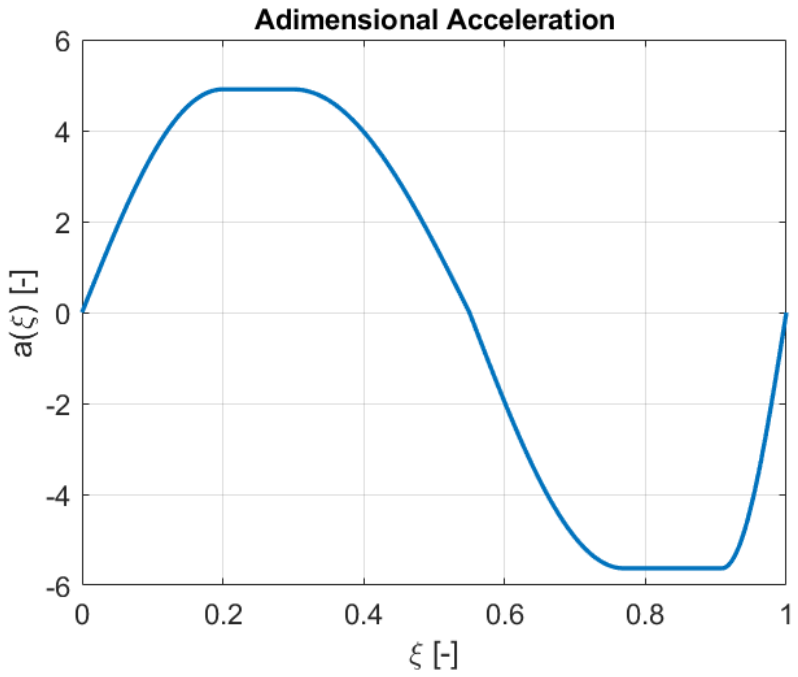

Figure 2.4: Adimensional Acceleration First Motion Law

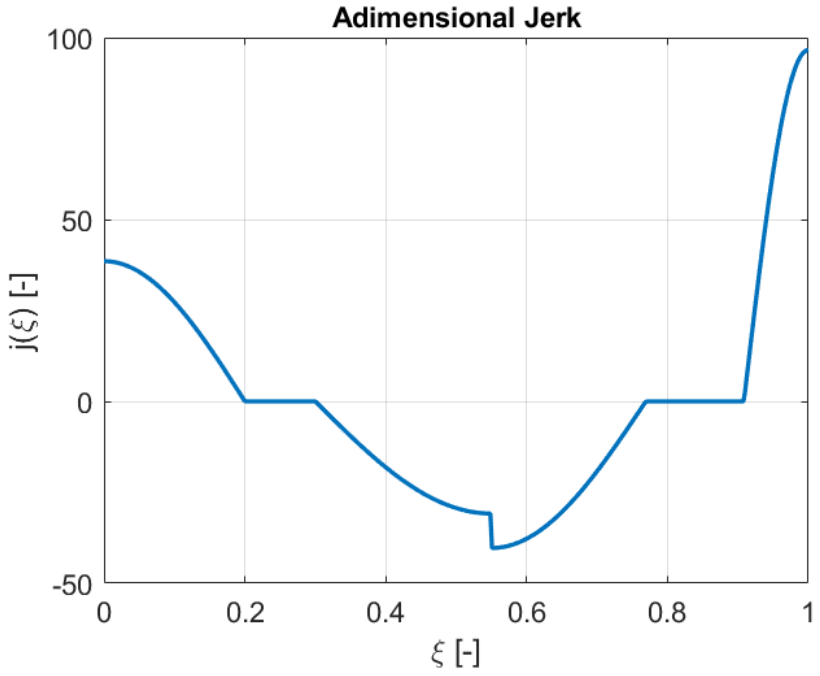

Figure 2.5: Adimensional Jerk First Motion Law

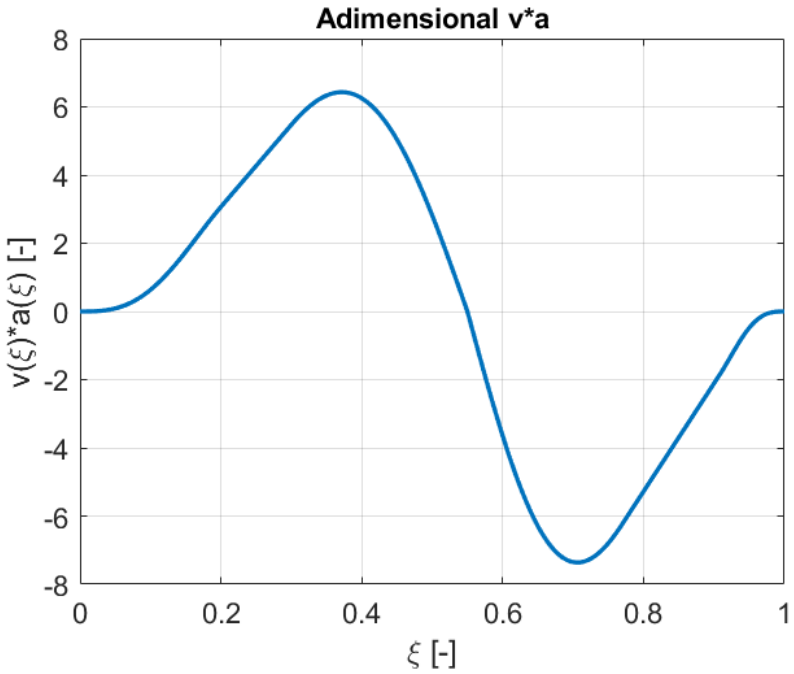

Figure 2.6: Adimensional V*A First Motion Law

2.3 Design Second Motion Law

In table 2.3 the motion law specifications for the rotation of the uploading arm are reported. Also in this case the rise and fall are kept symmetric; thus, only the rise phase is discussed.

$\alpha[^\circ]$	$\theta[^\circ]$	Phase
0	0	Dwell
100	0	Rise
130	90	Dwell
170	90	Fall
200	0	Dwell
360	0	

Table 2.3: Motion Law Specifications θ

The same criteria used for the choice of the first motion law are valid for the second motion law. In this case there is no need to pass through intermediate points; thus, in order to keep the problem simple, a family of motion laws including the cycloidal one is taken into consideration. Indeed, the cycloidal motion law can be seen as a particular case of modified trapezoidal law having fractions of the rise angle:

$$\frac{\delta}{\alpha_s} = \begin{bmatrix} d_1 & 0.0 & 0.5 - d_1 & 0.0 & 0.5 - d_1 & 0.0 & d_1 \end{bmatrix}$$

with $d_1 = 0.25$.
In figure 2.7 and 2.8 plots showing the dependency of the main performance parameters on the choice of d_1 are depicted, where the magenta dot stands for the cycloidal motion law case. It is illustrated that decreasing d_1 all the performance parameters are improved, but when d_1 approaches zero the jerk goes to infinity. It is evident that the best value for d_1 is the one for which the performance parameters are the smallest possible and at the same time the jerk is not too high.
Another effect due to the choice of d_1 is represented in figure 2.9: the smaller d_1 the higher the final pressure angle of the second cam given the same motion law for the first cam and the same design parameters for the second cam. Moreover, it has been noticed that the undercut problem is worsened as d_1 is reduced.
In the end, cycloidal law is chosen in order to satisfy the trade-off between the two impacts of varying d_1. This selection also features the smallest possible jerk. The performance parameters of the cycloidal motion law are reported in table 2.4.

c_v	c_a^+	c_a^-	c_k
2.0	6.28	6.28	8.13

Table 2.4: Performance Parameters First Motion Law

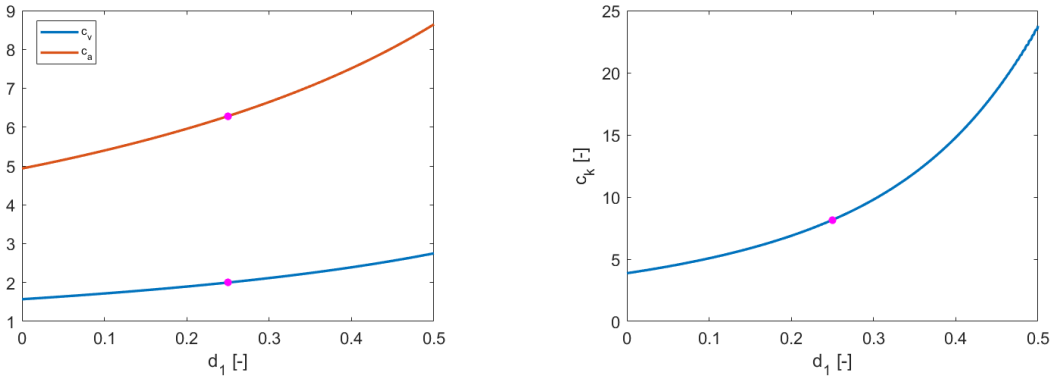

Figure 2.7: Left: c_v and c_a dependency on d_1; Right: c_k dependency on d_1.

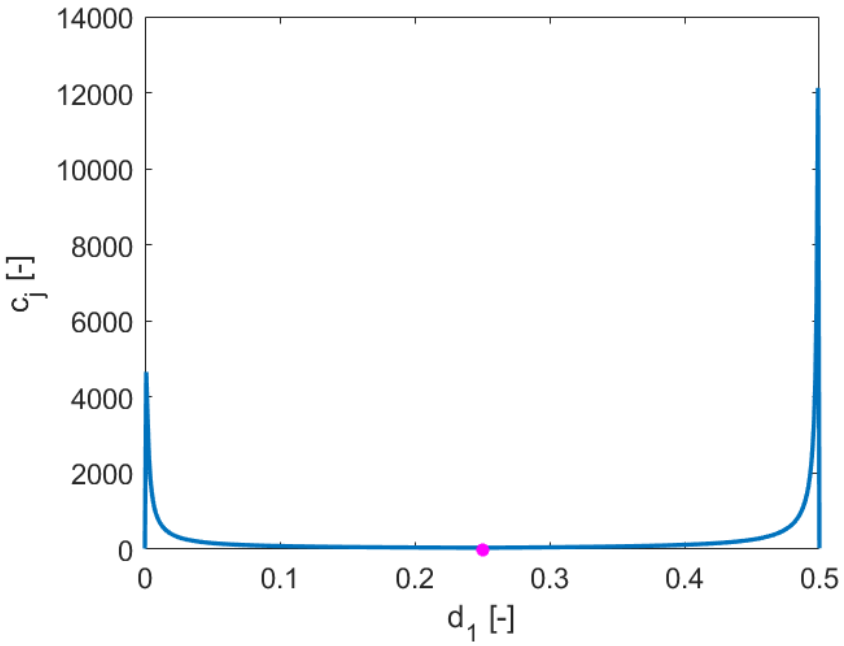

Figure 2.8: Dependency of Maximum Jerk on d_1

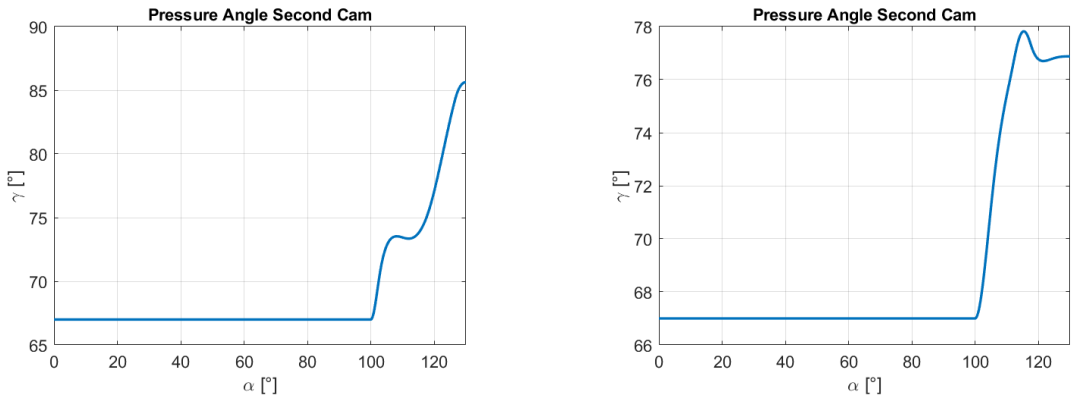

Figure 2.9: Left: pressure angle trend of Second Cam with $d_1 = 0.1$; Right: pressure angle trend of Second Cam with $d_1 = 0.4$.

3 Cams Synthesis

3.1 Synthesis First Cam

The first cam is a negative cam because, as it can be seen in figure 1.2, the x positive direction points towards the cam itself. Moreover, due to the big forces which are exchanged in the second cam, the first cam is chosen to be form closed (grooved).

The parameters which have to be chosen for the synthesis of the first cam are:

1. The roller radius R_r of the first follower (the slider): the roller radius influences both the contact pressure and the presence of undercuts. A roller radius that is too large diminishes the contact pressure while possibly introducing undercut depending on the base radius' size. Viceversa, a roller radius that is too small increases the contact pressure while reducing the probability of having undercuts. Thus, a reasonable trade-off value should be chosen.

2. The thickness of the cam b: looking only at the mathematical formulas, it seems that the larger is b, the smaller is the contact pressure without any drawback. But actually when b is too big there is a higher probability of having misalignments. A misalignment would result in a smaller contact surface and this would lead to larger contact pressures. Moreover, the thicker the cam the heavier and more expensive is the mechanism. In the end, also the choice of b needs a compromise.

3. The maximum and minimum pressure angles allowed γ_{max} and γ_{min}, respectively: when a force closed cam is used, the force transmitted from cam to follower points towards the follower, implying that friction represents a further limit to the pressure angle only during the rise phase; but in a grooved cam, for both the motions the roller is in contact with the internal or the external wall of the cam, thus the force transmitted is always opposite to the friction. In the end, it is reasonable to choose $\gamma_{max} = \gamma_{min} = 30°$.

4. The eccentricity desired e. The eccentricity is usually used in order to reduce the maximum pressure angle that occurs during operation since, as aforementioned, in force closed cams $\gamma_{max} < \gamma_{min}$. In the case of a grooved cam the two limits are exactly the same, thus the eccentricity chosen is $e = 0$.

Once the listed parameters have been selected and having already designed the first motion law, the cam can be generated in order to have the smallest possible base radius R_{b0} which allows to fulfill the limits for the pressure angle and to avoid the undercut. In table 3.1 the final choice of the design parameters for the first cam are summarized. In figure 3.1 the cam profiles obtained are depicted and in figure 3.2 the trend of the pressure angle of the cam is shown. The resulting size index of the cam is $R/h = 2.54$.

$R_r[mm]$	$b[mm]$	$\gamma_{max}[^\circ]$	$\gamma_{min}[^\circ]$	$e[mm]$	$R_{b0}[mm]$
20.0	20.0	30	30	0.0	368.0

Table 3.1: Design Parameters First Cam

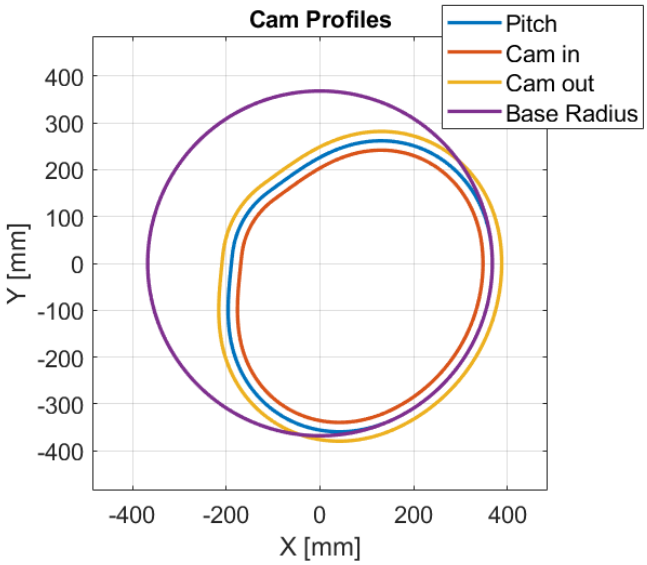

Figure 3.1: First Cam Profiles

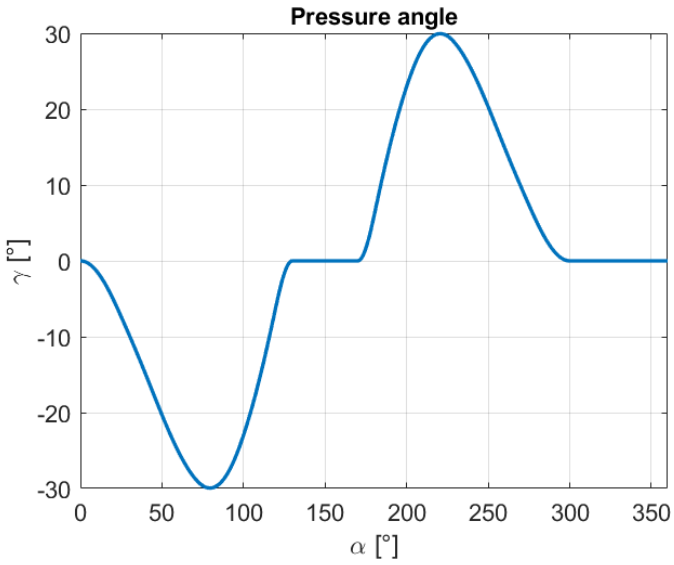

Figure 3.2: Pressure Angle First cam

3.2 Synthesis Second Cam

3.2.1 Design Parameters

In addition to the two motion laws previously discussed, the second cam needs the choice of four design parameters in order to be generated. Referring to figure 3.3, the design parameters needed can be easily identified:

1. The red circle is the roller having radius R_r. This has to be chosen taking into account the undercut problem and the contact pressure.
2. The angle between the green vertical line and the yellow sloped line is β_0, the initial angular position of the follower.
3. The magenta body is the follower link having length l.
4. The cam thickness b which affects the contact pressure and the misalignment problems.

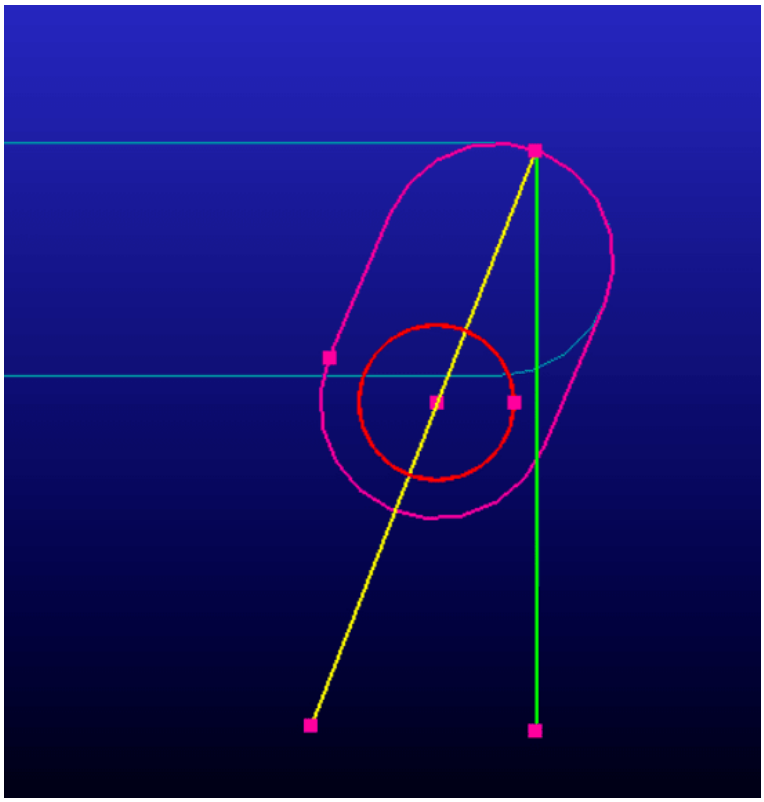

Figure 3.3: Parameters for Second Cam Synthesis

It is clear what the roller radius R_r and the cam thickness b affect, not the same can be said for β_0 and l. In the following subsection a study is performed in order to understand and show how β_0 and l influence the design.

3.2.2 Influence of β_0 and l on Cam Design

In figure 3.4 an example of the pressure angle of the second cam is shown during the rise phase, that is from $\alpha = 0°$ to $\alpha = 130°$:

1. Till $\alpha = 100°$ the pressure angle remains constant and equal to $90° - \beta_0$, where here $\beta_0 = 23°$.
2. From $\alpha = 100°$ to $\alpha = 130°$ the pressure angle changes and it is desired to keep it as small as possible.

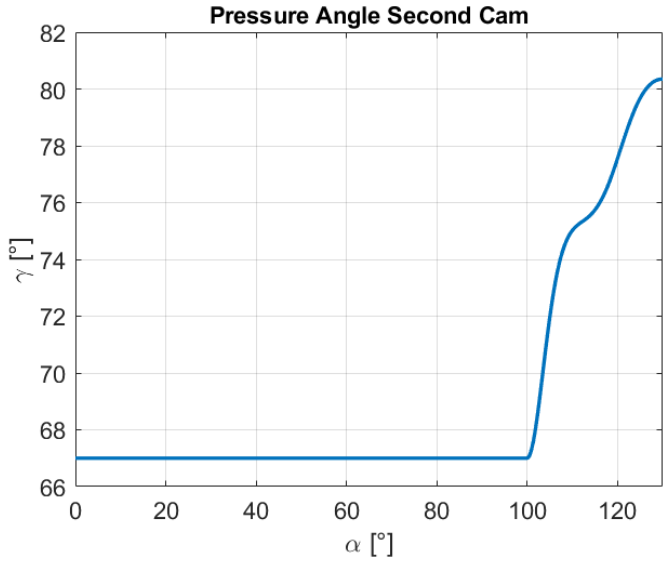

Figure 3.4: Example trend Pressure Angle Second Cam

Therefore, it is studied how β_0 and l affect the initial and final pressure angle of the second phase described above ($\alpha \in [100°, 130°]$). In figures 3.5 and 3.6 the result of this study is shown for the initial and final pressure angle, respectively:

- As previously mentioned, the initial pressure angle is the complementary of β_0, thus it does not depend on the link length l. Using a vertical initial position of the follower ($\beta_0 = 0°$), the initial pressure angle is 90° and this makes the rotation of the follower unfeasible. Thus, a vertical or almost vertical initial position of the follower is discarded while a horizontal or close to horizontal initial position looks like the most suitable option thus far.
- Looking at the plot of the final pressure angle, it is realized that an initial position close to the horizontal would create problems at the end of the rise phase since the pressure angle would take a value close to 90° independently of the link length. Moreover, the plot shows also that the smaller l, the better the final pressure angle.

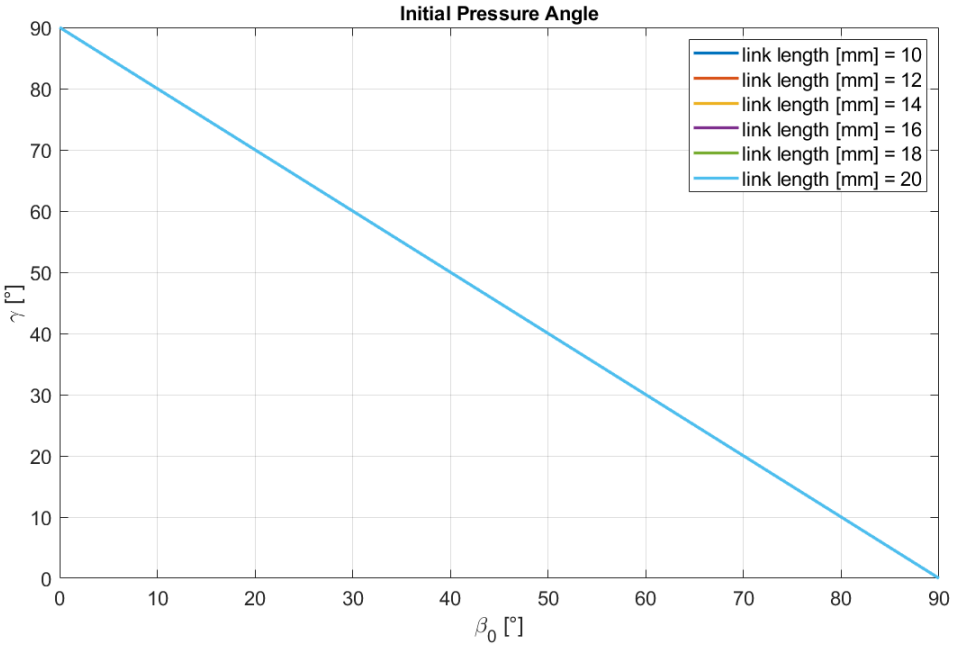

Figure 3.5: Initial Pressure Angle of Second Cam as function of β_0 and l

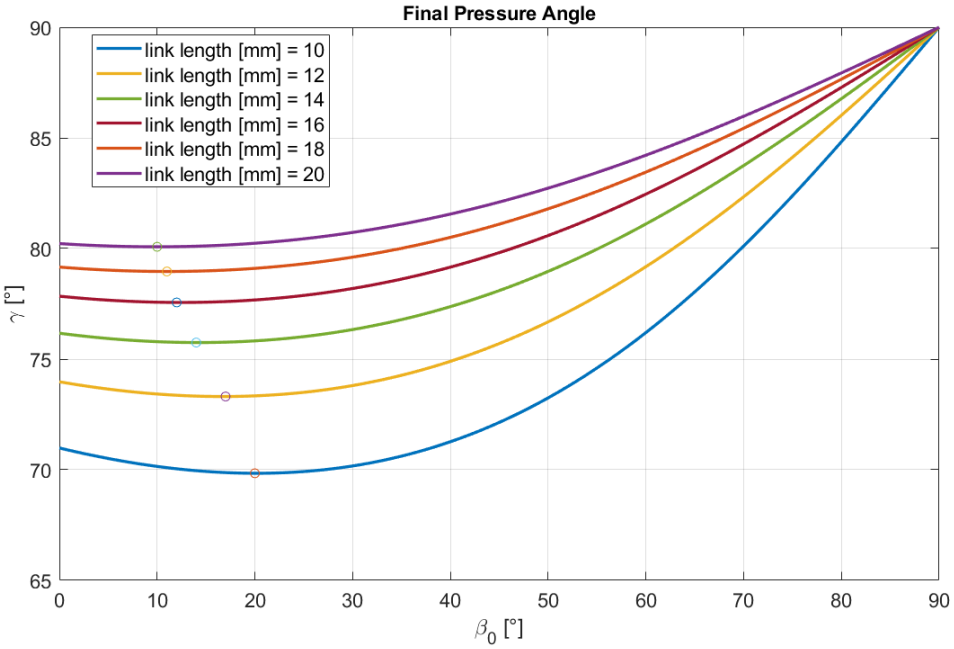

Figure 3.6: Final Pressure Angle of Second Cam as function of β_0 and l. The circles correspond to the minimum of each curve.

3.2.3 Design Parameters Choice

As a result of the analysis carried out in subsection 3.2.2, β_0 should be chosen trying to keep as far as possible both initial and final pressure angle from 90°, while l should be chosen to be as small as possible. A lower limit to l is provided by analyzing the undercut problem, which becomes worse as it decreases. The final values chosen for the synthesis of the second cam are reported in table 3.2 and the second cam profile obtained is shown in figure 3.7. The pressure angle trend obtained is the same shown in figure 3.4.

$R_r[mm]$	$b[mm]$	$\beta_0[°]$	$l[mm]$
10.0	20.0	23	20.0

Table 3.2: Design Parameters Second Cam

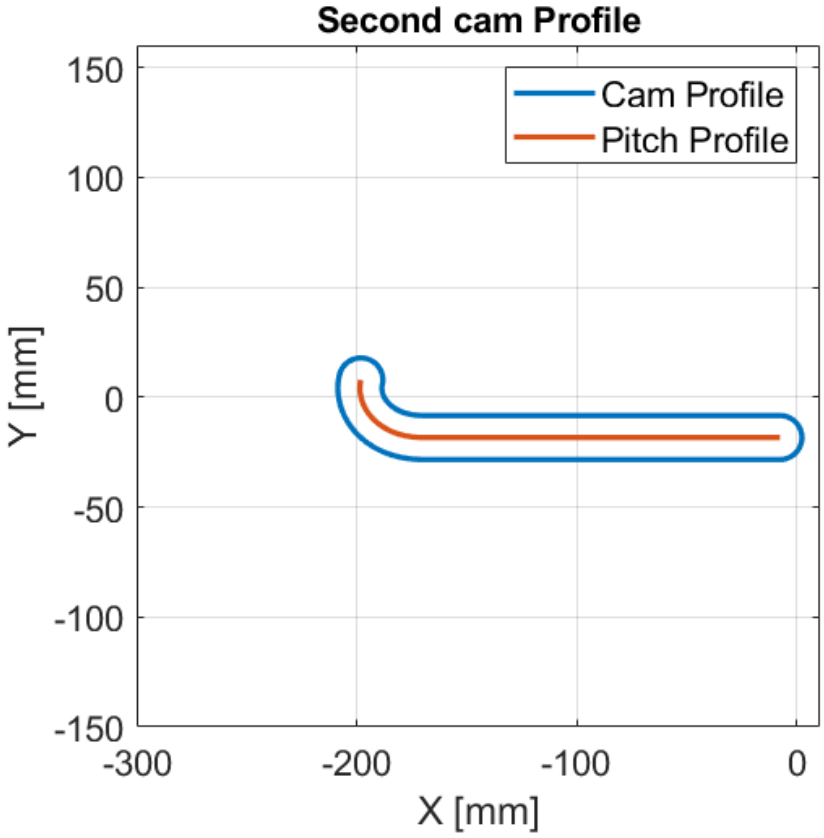

Figure 3.7: Second Cam Profile

4 Adams Model and Simulation Analysis

4.1 Introduction

The mechanism is assembled and tested using the software MSC Adams. The chapter is organized as follows:

1. Description of the model in all its parameters which are mainly the sizes of the components and their inertial characteristics.
2. Kinematic analysis of the mechanism: here the motion applied to the cam is ideal and the rollers' centers of the two followers are constrained to move along the pitch profiles of the cams. This analysis is useful to check if the mechanism designed works kinematically and to compute the feed-forward torque to be applied by the motor.
3. Dynamic analysis of the mechanism: here real forces are applied (contacts, torques etc.) and the mechanism is simulated and verified in its real dynamical behaviour.

4.2 Model Description

In figure 4.1 the model drawn using the software MSC Adams is depicted. The following assumptions have been made:

1. The first cam is optimized in terms of mass distribution and its center of mass is located along its rotational axis. Since the speed of the cam is constant, its inertial characteristics do not play any role in the analysis.
2. The total mass of the slider is distributed between the first roller ($0.2kg$) and the first follower ($4.3kg$).
3. The uploading arm has not been drawn, simply its mass and inertia, respectively $1.2kg$ and $0.5kgm^2$, are distributed between the second follower and the second roller.
4. The second cam is grounded so its inertial features do not play any role in the analysis.

All relevant sizes of the components have already been specified in chapter 3.

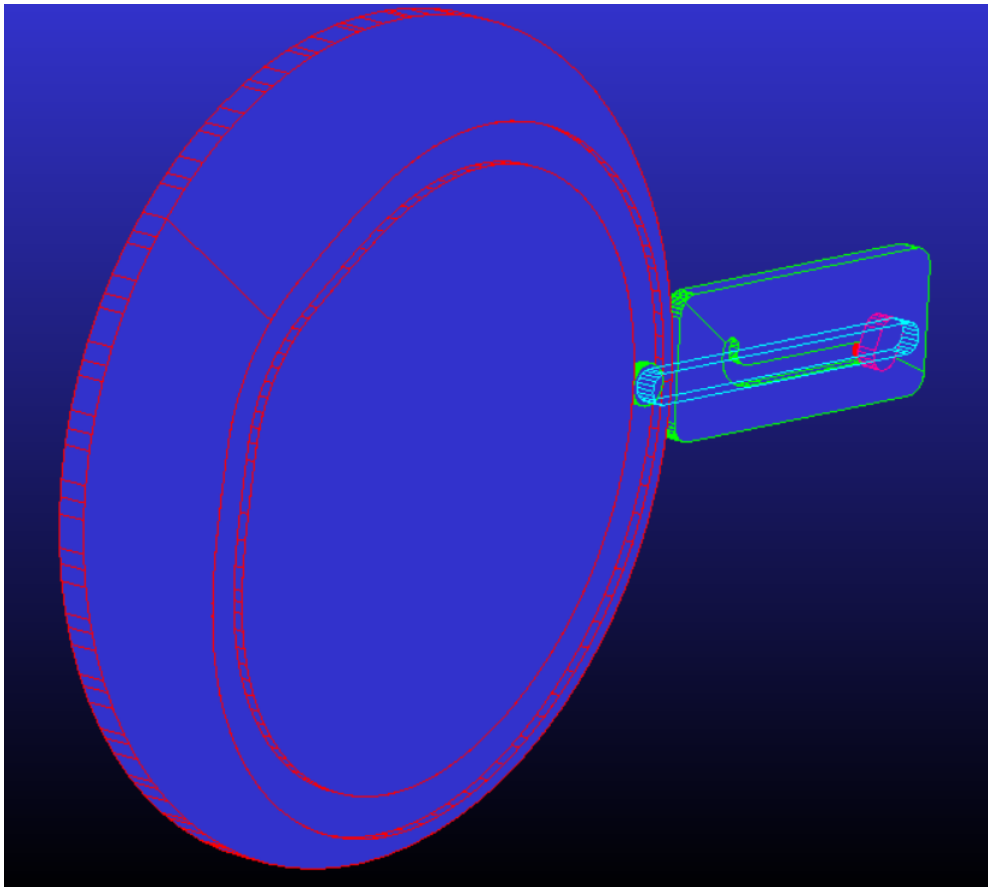

Figure 4.1: MSC Adams Model

4.3 Kinematic Analysis

Point to curve constraints are applied between the center of the rollers and the pitch profiles of the cams, and an ideal motion starting directly from the steady-state condition is imposed to the first cam. The simulation lasts 2 seconds so that one full rotation is completed. In figures 4.2 and 4.3 the comparison between the result of the kinematic analysis and the designed motion laws is shown respectively for first and second follower, while in figure 4.4 the torque applied to the first cam for ensuring the motion imposed is displayed. It can be concluded that the mechanism is kinematically verified.

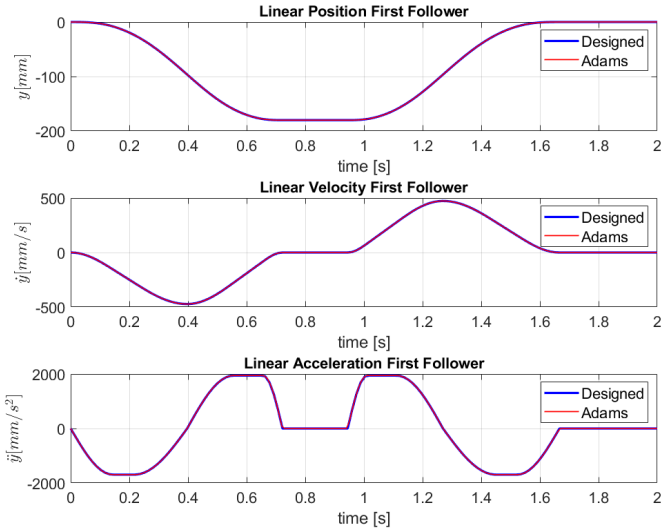

Figure 4.2: Comparison between designed motion law and motion law obtained from kinematic analysis using MSC Adams for the first follower

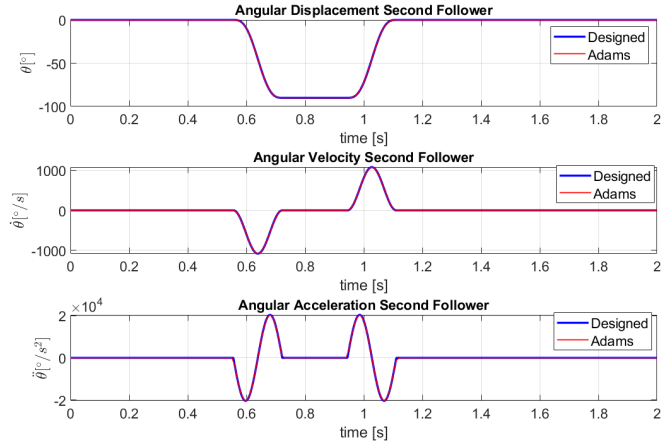

Figure 4.3: Comparison between designed motion law and motion law obtained from kinematic analysis using MSC Adams for the second follower

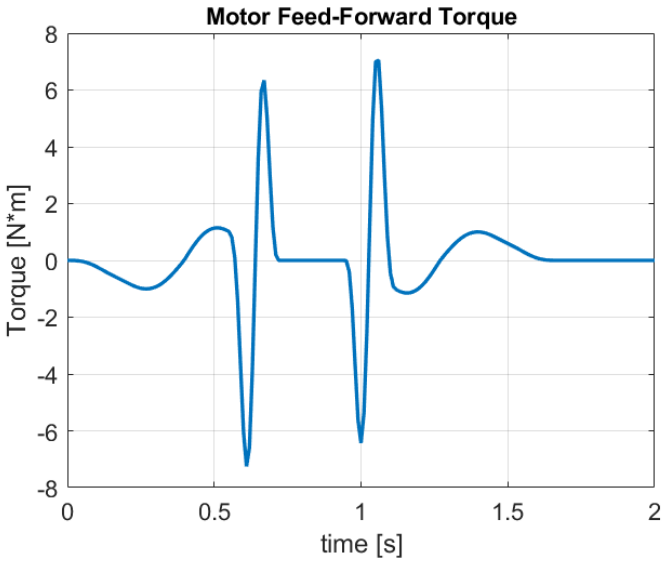

Figure 4.4: Feed-Forward Torque

4.4 Dynamic Analysis

In the dynamic analysis all the ideal constraints are replaced with real forces or torques and the real dynamic behaviour of the mechanism is analyzed.

4.4.1 Real contacts

In order to obtain a dynamic model, all the ideal point to curve constraints have been replaced with real contacts between rollers and cams. The material selected for the bodies of the model is steel, moreover no lubricant is used in the machine in order to avoid contamination of the soap. Therefore, the contact type dry steel-steel is employed in the model, the parameters of which are reported in figure 4.5.

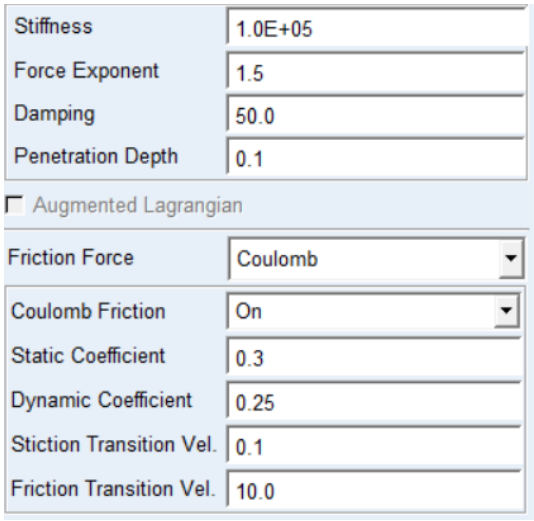

Figure 4.5: Contact Parameters

4.4.2 Motor Torque

The ideal motion of the cam is removed and the real torque is added. The torque formulation is written in equation 4.1.

$$\tau_d = \tau_{ff} + k_p(\alpha^* - \alpha) + k_d(\omega^* - \omega) \tag{4.1}$$

where τ_d is the desired torque, τ_{ff} is the feed-forward torque derived from the kinematic analysis, k_p and k_d are respectively proportional and derivative gain of the feed-back PD control done on the position of the cam. If the system is simulated without external disturbances the feed-forward term should be enough to reproduce the same motion shown in the kinematic analysis. However, due to numerical errors the feed-back contribution is necessary even without external disturbances. It is used $k_p = k_d = 1e06$.

4.4.3 First Dynamic Analysis

The results obtained in terms of motion laws are reported in figures 4.6 and 4.7, while the contact forces are shown in figures 4.8 and 4.9.

Results Comment By analyzing the acceleration plots it can be concluded that after the rise phase the second follower starts vibrating and these vibrations are even more evident during the fall phase and are transmitted to the first cam. Indeed, analyzing the contact forces of the two cams it can be understood that both the rollers are bouncing inside the grooves of their respective cams. This outcome is not acceptable; therefore, a second dynamic analysis is carried out adding a torsional spring in the revolute joint between the slider and the second follower with the goal of reducing its oscillations.

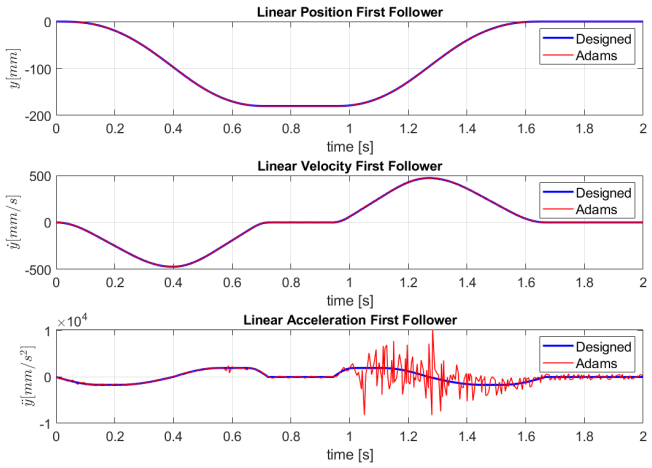

Figure 4.6: Dynamic Analysis Motion Laws Slider

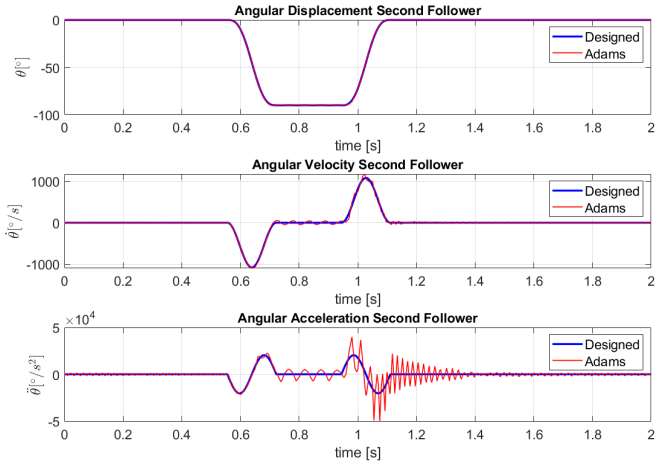

Figure 4.7: Dynamic Analysis Motion Laws Second Follower

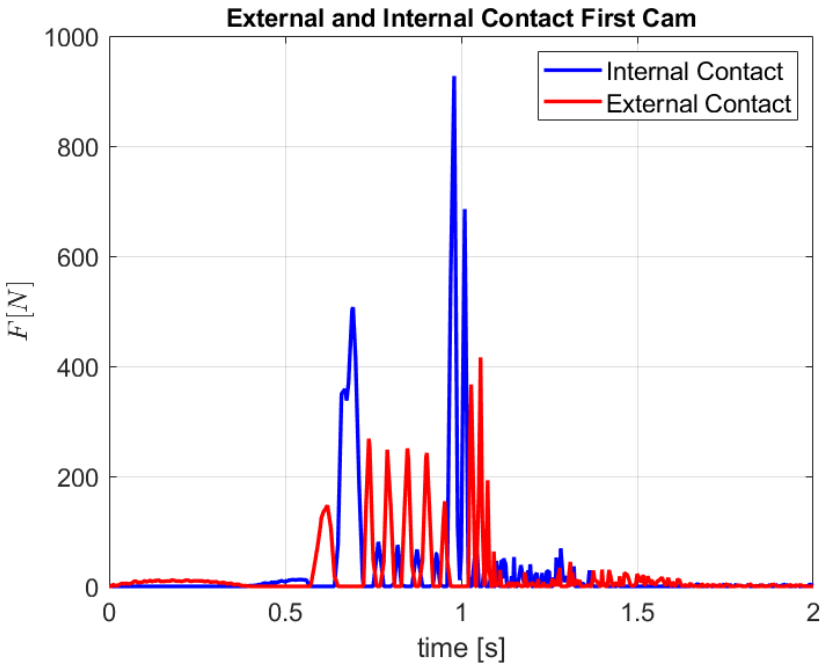

Figure 4.8: External and Internal Contact First Cam

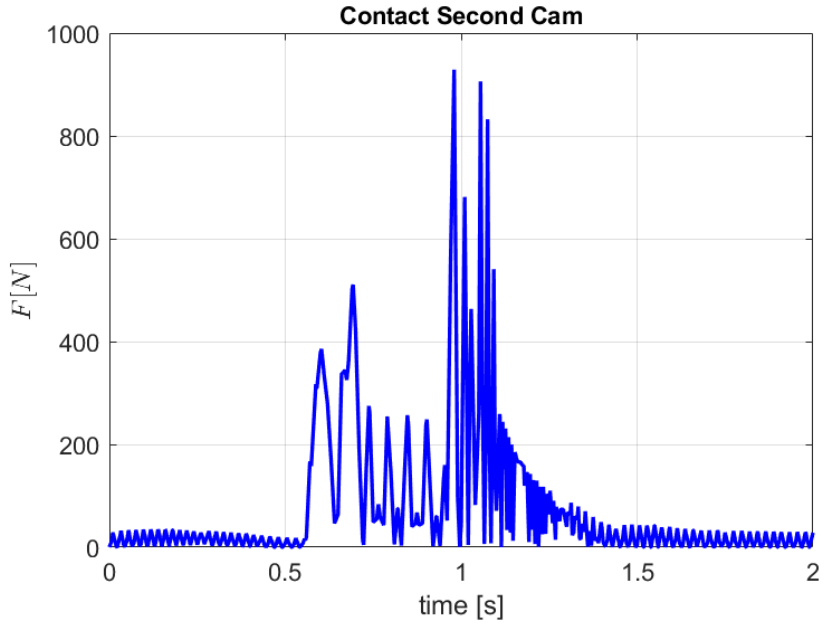

Figure 4.9: Contact Second Cam

4.4.4 Second Dynamic Analysis

Now a torsional spring is integrated in the system, located in the revolute joint between the slider and the link of the rotating follower. The torsional spring should keep the second follower pressed against the lower part of the second cam helping to avoid its incessant bouncing.

Torsion Spring Selection The torsion spring is selected from the catalogue of the manufacturer LeeSpring. For sake of simplicity it is assumed that the revolute joint where the spring has to act has been designed so that the correct mounting of the spring is allowed. Moreover, since a preload is needed, the spring is selected among the springs which can reach 180° deflection and it is assumed that the spring is mounted pre-deflected of 90°. In figure 4.10 it is reported the page of the aforementioned catalogue used for the selection of the torsion spring.

TORSION SPRINGS: 180° FREE POSITION *(INCH)*

*Music Wire (Plated**) or 302 Stainless Steel* (Passivated) or 316 Stainless Steel (Passivated Ultrasonically Cleaned),*
LTL - Left Hand Wound; LTR - Right Hand Wound

LEE STOCK NUMBER	OUTSIDE DIAMETER		WIRE DIAMETER		TORQUE @ 180° DEFLECTION (T) (See Footnote)		RADIUS (R)		SUGGESTED MANDREL SIZE		LENGTH OF LEG (A)		BODY LENGTH APPROX.(L)		NUMBER OF COILS	PRICE GROUP		
																Music Wire	302 Stainless*	316 Stainless
	IN.	MM	IN.	MM	IN.-LB.	KG-MM	IN.	MM	IN.	MM	IN.	MM	IN.	MM		M	S	S316
LTL070M 04 LTR070M 04	.810	20.57	.070	1.78	7.500	86.41	1.000	25.40	19/32 (.594)	15.08	2.000	50.80	0.500	12.70	6.00	Z	AA	SPECIAL ORDER
LTL085N 04 LTR085N 04	.891	22.63	.085	2.16	12.861	148.18	1.250	31.75	41/64 (.641)	16.27	2.500	63.50	0.694	17.63	7.00	AB	AC	SPECIAL ORDER
LTL095P 02 LTR095P 02	.920	23.37	.095	2.41	17.148	197.57	1.500	38.10	21/32 (.656)	16.67	3.000	76.20	0.872	22.15	8.00	AB	AC	SPECIAL ORDER
LTL105Q 02 LTR105Q 02	.982	24.94	.105	2.67	21.000	241.95	1.750	44.45	45/64 (.703)	17.86	3.500	88.90	1.050	26.67	9.00	AC	AD	SPECIAL ORDER
LTL095P 04 LTR095P 04	1.038	26.37	.095	2.41	17.148	197.57	1.500	38.10	49/64 (.766)	19.45	3.000	76.20	0.775	19.69	7.00	AB	AC	SPECIAL ORDER
LTL115R 02 LTR115R 02	1.043	26.49	.115	2.92	28.000	322.60	2.000	50.80	47/64 (.734)	18.65	4.000	101.60	1.150	29.21	9.00	AD	AE	SPECIAL ORDER
LTL125S 02 LTR125S 02	1.082	27.48	.125	3.18	32.000	368.69	2.000	50.80	49/64 (.766)	19.45	4.000	101.60	1.500	38.10	11.00	AE	AG	SPECIAL ORDER
LTL135T 02 LTR135T 02	1.189	30.20	.135	3.43	40.000	460.86	2.000	50.80	27/32 (.844)	21.43	4.000	101.60	1.620	41.15	11.00	AG	AJ	SPECIAL ORDER
LTL105Q 04 LTR105Q 04	1.248	31.70	.105	2.67	21.000	241.95	1.750	44.45	15/16 (.938)	23.81	3.500	88.90	0.840	21.34	7.00	AD	AE	SPECIAL ORDER
LTL115R 04 LTR115R 04	1.348	34.24	.115	2.92	28.000	322.60	2.000	50.80	1 (1.000)	25.40	4.000	101.60	0.920	23.37	7.00	AE	AG	SPECIAL ORDER
LTL125S 04 LTR125S 04	1.356	34.44	.125	3.18	32.000	368.69	2.000	50.80			4.000	101.60	1.125	28.58	8.00	AG	AJ	
LTL135T 04 LTR135T 04	1.491	37.87	.135	3.43	40.000	460.86	2.000	50.80	1 3/32 (1.094)	27.78	4.000	101.60	1.215	30.86	8.00	AJ	AK	SPECIAL ORDER

Figure 4.10: Torsion Spring Catalogue, LeeSpring

The torsional stiffness of the spring is computed using equation 4.2.

$$k_T = \frac{T}{180} \tag{4.2}$$

where T is the torque exerted by the spring when it is deflected of 180°, expressed in $[Nmm]$. Then, the preload is computed as $P = 90k_T$ where k_T is expressed in $[Nmm/°]$.

After having performed some dynamic simulations, the smallest spring for which the undesirable bouncing disappears is the number $L085N04$ having $P = 726.5Nmm$ and $k_T = 8.07Nmm/°$.

Motor Torque The feed-forward torque used previously is again implemented due to the fact that the feed-back contribution allows to compensate for the eventual external disturbances introduced by the torsional spring.

Motion Laws and Contact Forces The results obtained in terms of motion laws are reported in figures 4.11 and 4.12, while the contact forces are shown in figures 4.13 and 4.14.

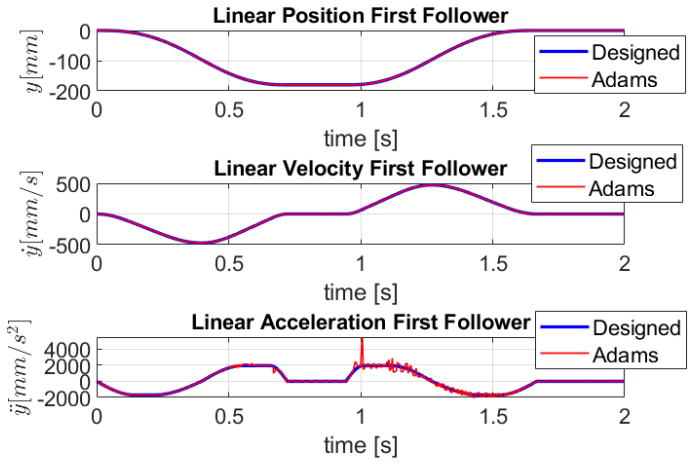

Figure 4.11: Dynamic Analysis Motion Laws Slider with Torsional Spring

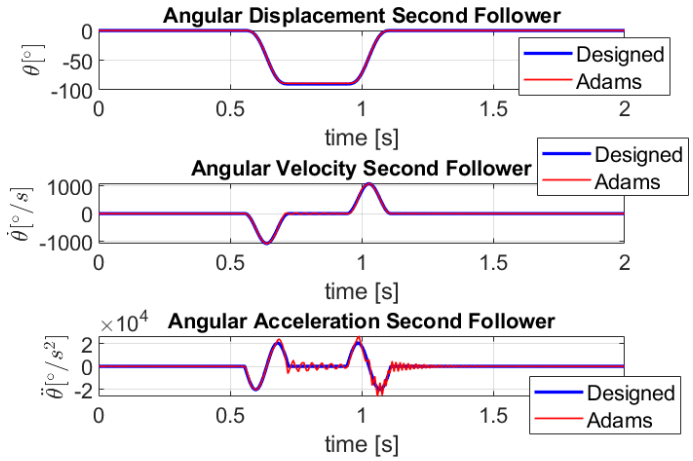

Figure 4.12: Dynamic Analysis Motion Laws Second Follower with Torsional Spring

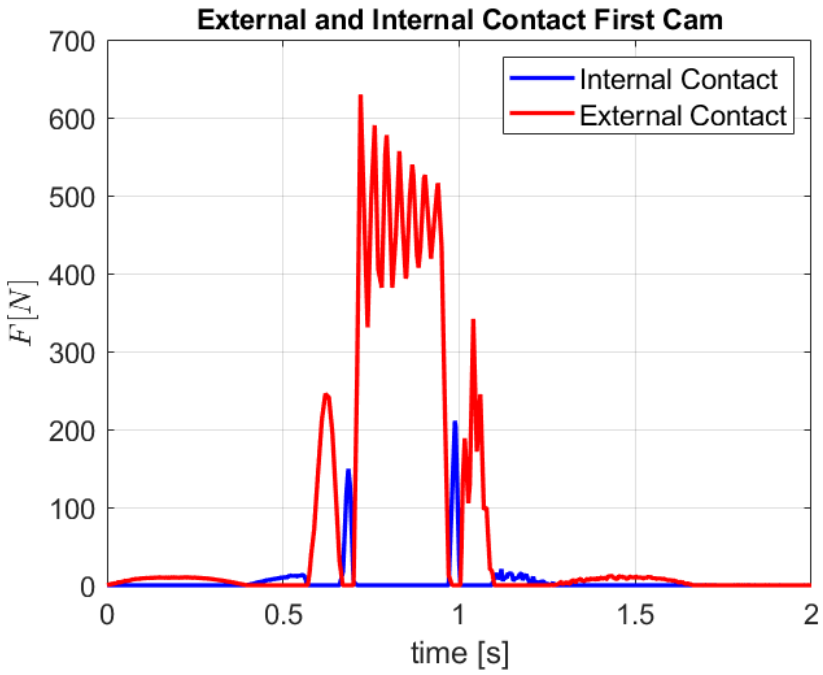

Figure 4.13: External and Internal Contact First Cam with Torsional Spring

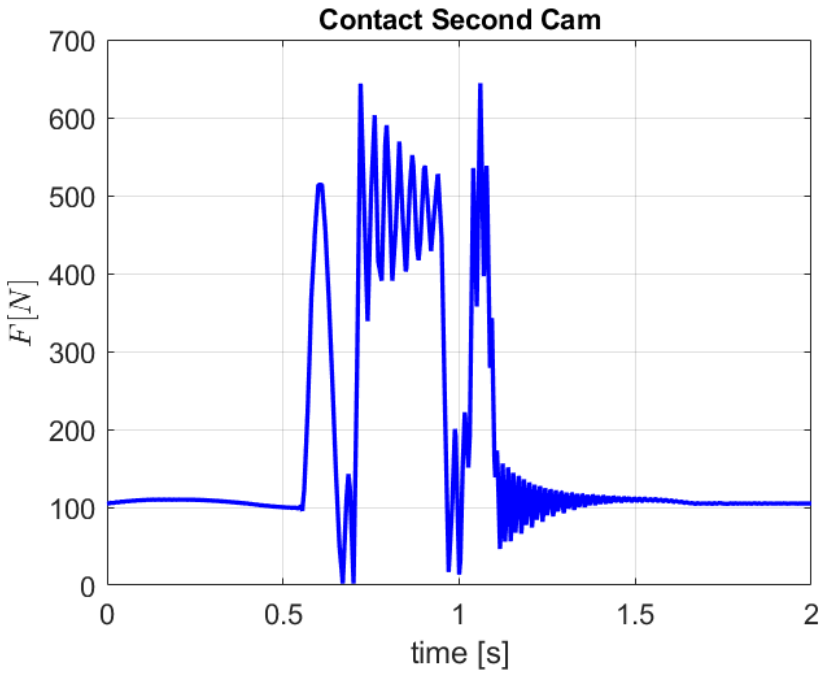

Figure 4.14: Contact Second Cam with Torsional Spring

Vibrations are still present in the system but an evident improvement is obtained, which makes the design acceptable. Snapshots of the main important instants of the simulation are here shown and explained:

1. Figure 4.15 depicts the instant when the rise of the second follower is starting, where the yellow arrows represent the contact forces that the cams apply on the rollers. This instant corresponds to the first peak of the first cam external contact and to the first peak of the second cam contact.

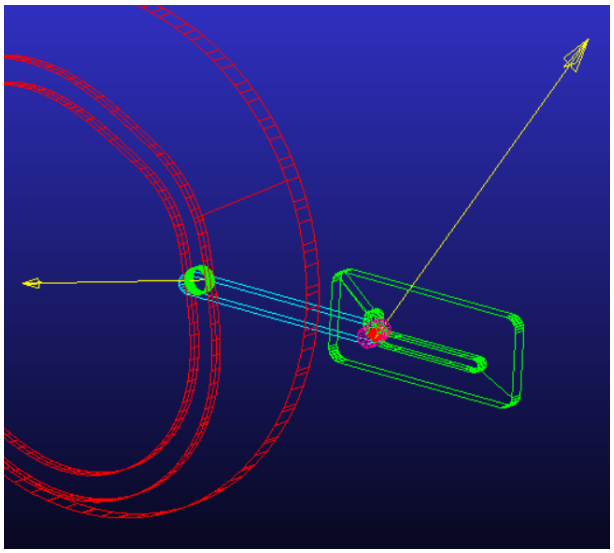

Figure 4.15: Phase 1 Simulation

2. In figure 4.16, almost at the end of the rise the roller goes in contact with the upper part of the second cam resulting in the peak of the first cam internal contact.

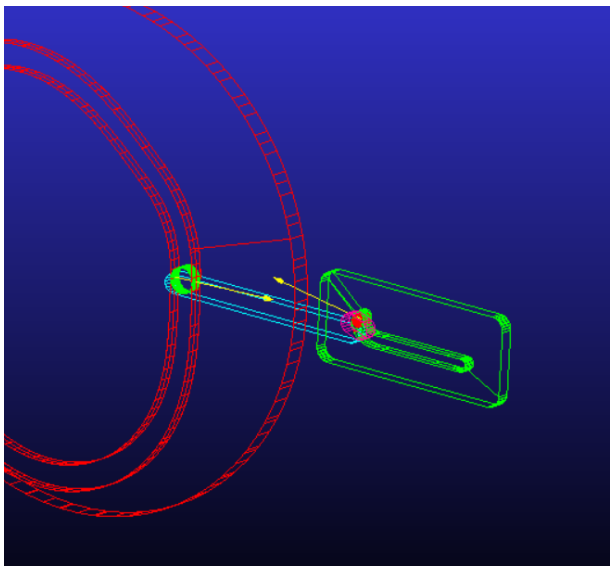

Figure 4.16: Phase 2 Simulation

3. In figure 4.17 during the dwell of the second follower the second roller remains in contact with the bottom part of the second cam thanks to the torsional spring, and consequently the first roller is in contact with the external profile of the first cam (wider peak in the two contact force plots).

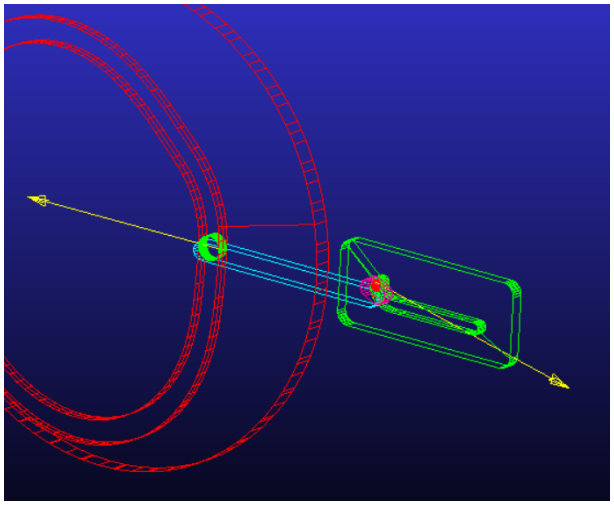

Figure 4.17: Phase 3 Simulation

4. In figure 4.18 the fall of the uploading arm is starting and the second roller hits the upper profile of the second cam resulting in the peaks of the first cam internal contact and of the second cam.

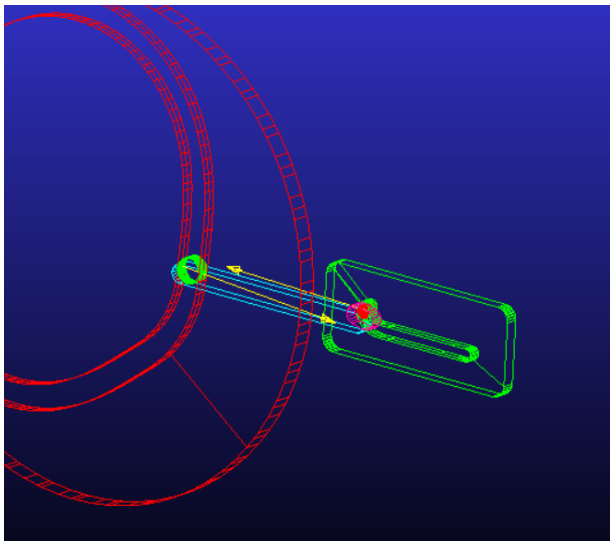

Figure 4.18: Phase 4 Simulation

5. In figure 4.19 the second roller goes again in contact with the bottom profile of the second cam and this causes the last peak of the first cam external contact. This last peak corresponding to an impact generates some oscillations for the remaining part of the motion law, which is when the second roller returns to its initial position.

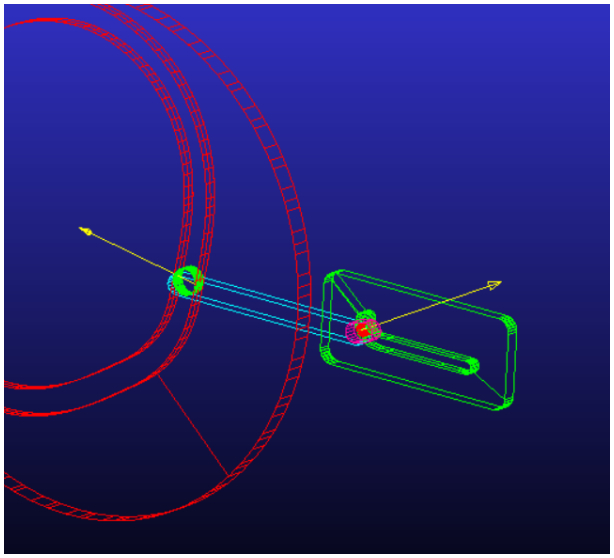

Figure 4.19: Phase 5 Simulation

Friction Analysis The friction is analysed and compared to the contact force multiplied by the static friction coefficient in order to understand if slippage occurs in the contact. In figures 4.20, 4.21 and 4.22 the comparison is performed for internal contact of first cam, external contact of first cam, and the contact of second cam, respectively. It can be concluded that since the friction plot is always below the maximum friction allowable, slippage never occurs.

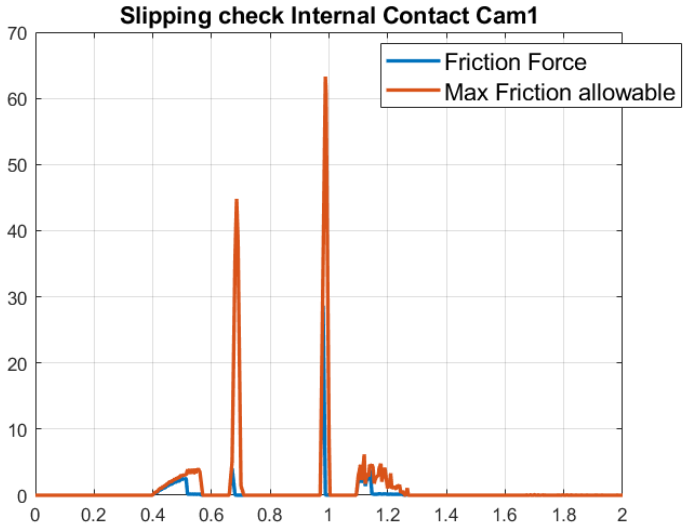

Figure 4.20: Slipping Check Internal Contact First Cam

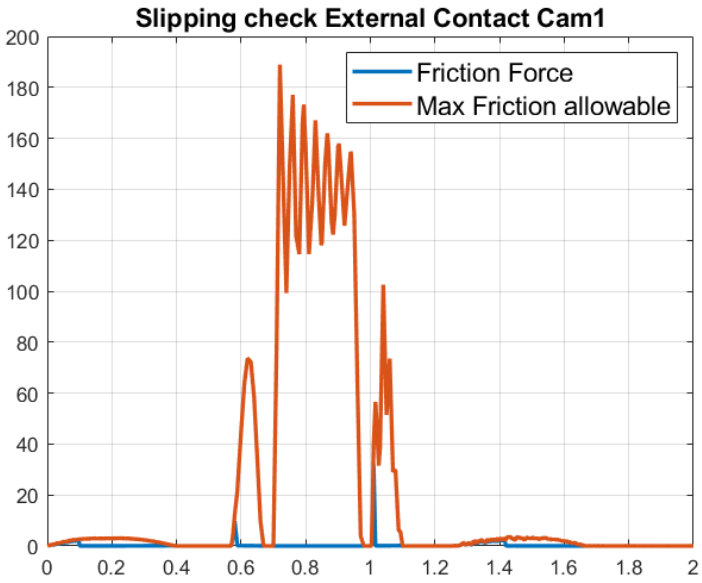

Figure 4.21: Slipping Check External Contact First Cam

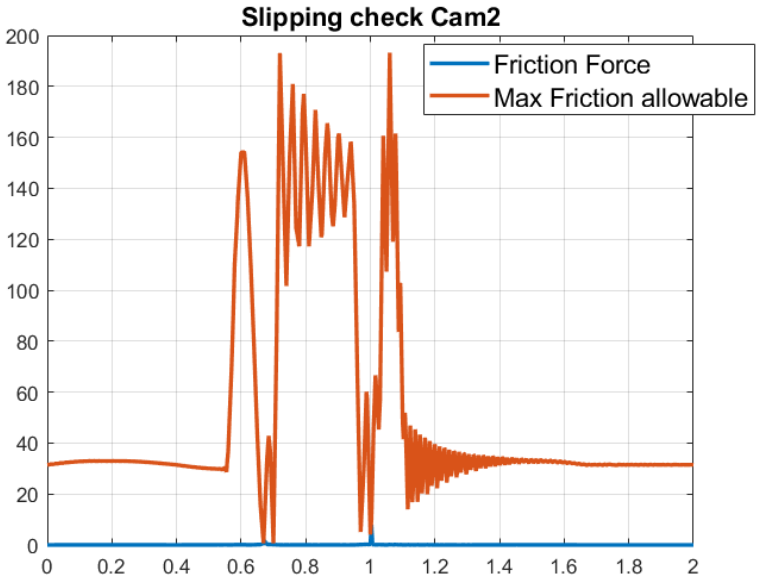

Figure 4.22: Slipping Check Contact Second Cam

Contact Pressure Check The contact pressure check consists in the assurance that the maximum contact pressure achieved is smaller than the allowable contact stress of the material chosen. Equation 4.3 is used for the computation of the contact pressure.

$$P = \sqrt{0.175 \frac{F_n E}{b R_r} (1 + \frac{R_r}{\rho})} \tag{4.3}$$

where F_n is the contact force, E is the Young Modulus of the material, b is the cam thickness, R_r is the roller radius and ρ is the curvature radius of the profile. All the parameters needed for contact pressure computation are available from dynamic analysis (F_n) and from cams synthesis except for the Young Modulus which is around $206000 MPa$ for steel. In figures 4.23, 4.24 and 4.25 the contact pressure trends are shown during one turn of the cam.

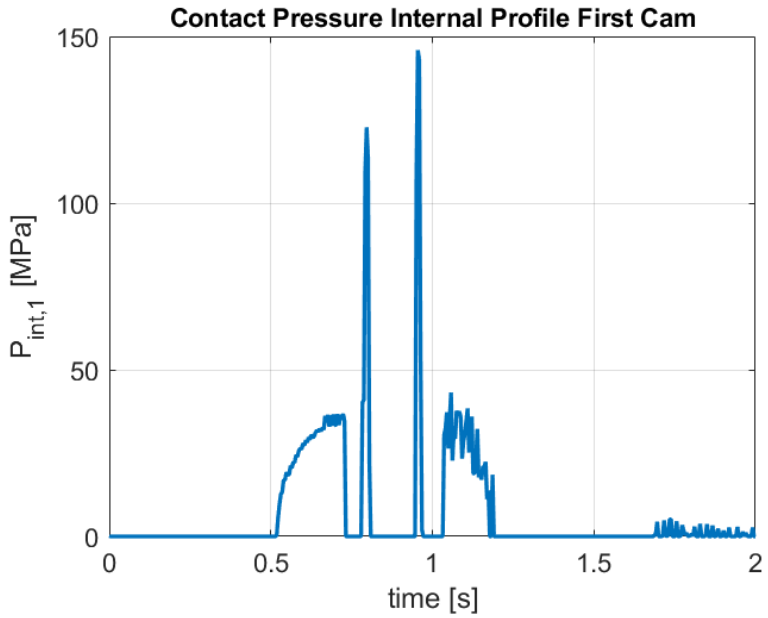

Figure 4.23: Contact Pressure Internal Profile First Cam

The maximum contact pressure achieved for the first cam is $P_{max,1} = 250 MPa$ and for the second cam is $P_{max,2} = 350 MPa$. Figure 4.26[1] shows how the allowable cam contact Herz stress changes as function of the cam hardness and of the material type. A wide range of materials can be selected since all those having a Brinnell Hardness higher than 150HB can satisfy the contact pressure check with a safety factor $\eta > 1.14$.

[1] `http://mechdesigner.support/contact-fatigue-cams-cam-followers.htm?toc=0&printWindow&`

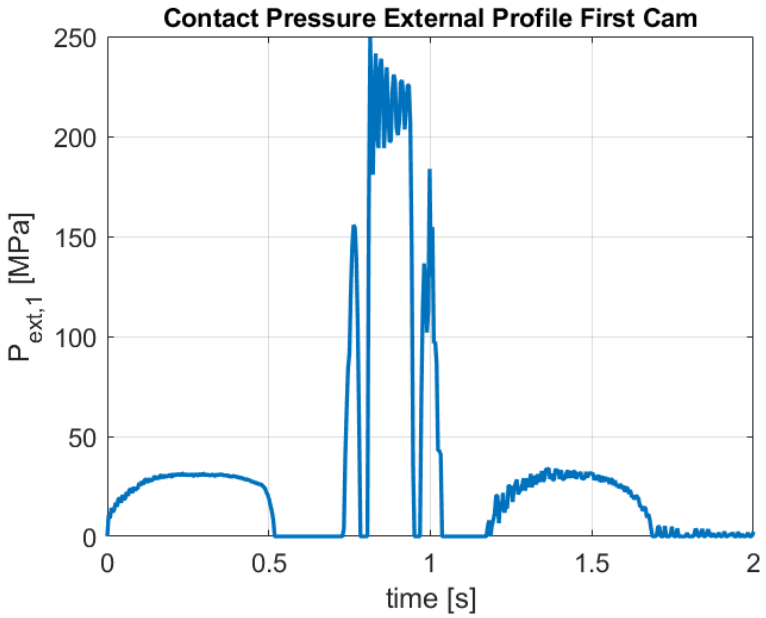

Figure 4.24: Contact Pressure External Profile First Cam

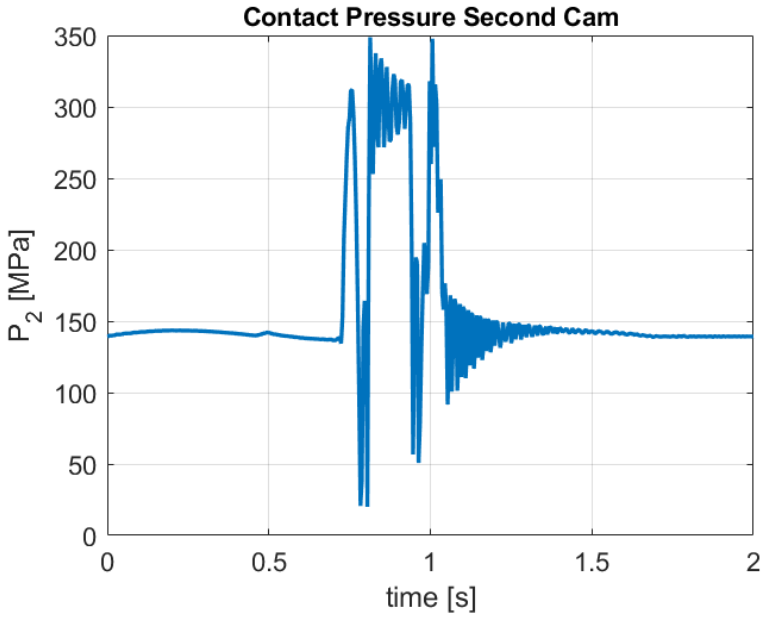

Figure 4.25: Contact Pressure Second Cam

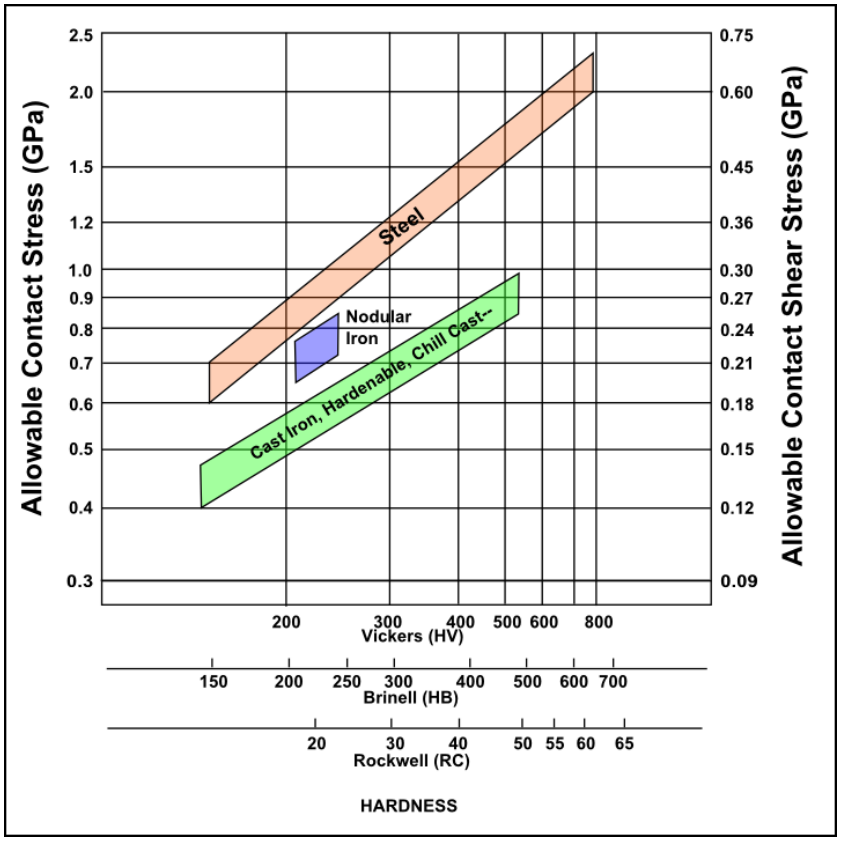

Figure 4.26: Cam Contact Hertz Stress as Function of Cam Hardness and Material Type

5 Motor Sizing

5.1 Requirements

The sizing of the motor is performed at steady-state condition, so no considerations on the inertias are done. The trend of the torque required, which has been obtained from the previous dynamic analysisis, is shown in figure 5.1 and its main parameters, useful for the motor dimensioning, are reported in table 5.1.

$T_{max}[Nm]$	$T_{RMS}[Nm]$	$\omega[rad/s]$
14.19	1.77	3.14

Table 5.1: Load parameters

The motor chosen together with the transmission should satisfy the following requirements:

1. The maximum torque demanded by the system (T_{max}) must be lower than the maximum output torque of the motor.
2. The root mean square torque demanded by the system (T_{RMS}) must be lower than the nominal torque of the motor.
3. The maximum speed demanded by the system (ω) must be lower than the maximum speed of the motor.

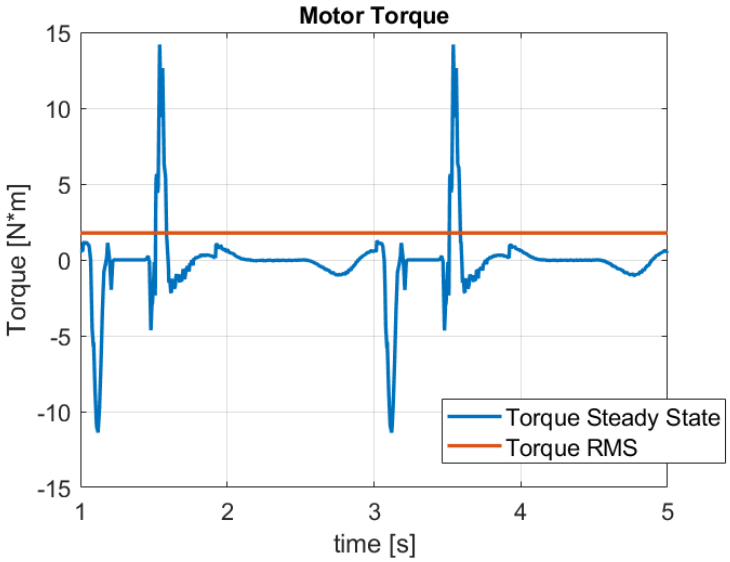

Figure 5.1: Torque demanded by the system

5.2 Choice of Transmission and Motor

In figure 5.2 a page of the catalogue of asynchronous motors used for the selection is shown. Both the nominal torque M_n and the maximum speed n are directly given in the catalogue, while the maximum torque or breakdown torque M_k can be computed from the ratio M_k/M_n using equation 5.1.

$$M_k = \frac{M_k}{M_n} M_n \tag{5.1}$$

By choosing the motor number $562C$, which significant parameters are reported in table 5.2, and a one stage gearbox having reduction ratio $i = 8$, the three requirements are satisfied as it is shown by the following calculations.

$$M_{k,load} = M_k i = 0.60 \cdot 3.1 \cdot 8 = 14.88Nm > T_{max}$$
$$M_{n,load} = M_n i = 0.60 \cdot 8 = 4.8Nm > T_{RMS}$$
$$n_{max,load} = \frac{n_{max}}{i} = \frac{2840}{8} = 355rpm = 5.92rad/s > \omega$$

$M_n[Nm]$	$M_k/M_n[Nm]$	$n[rpm]$
0.60	3.1	2840

Table 5.2: Parameters Motor Chosen

miksan MOTOR

ELECTRICAL VALUES: IE1 EFFICIENCY CLASS

TYPE	RATED OUTPUT		PERFORMANCE AT RATED OUTPUT							STARTING DATA		Breakdown Torque Ratio	Moment of interia	B3 Weight appx.
			Voltage		Speed	Current	Torque	Power Factor	Efficiency	Current Ratio	Torque Ratio			
	P_2		V		n	I_n	M_n	cos ø	η	I_s/I_n	M_s/M_n	M_k/M_n	J	
	kw	HP	Con.	V	rpm	A	Nm	-	%	-	-	-	kgm^2	kg
2 POLES- 3000 RPM														
56 2A	0.09	0.12	Δ/Y	230/400	2830	0.52/0.30	0.32	0.70	64.6	3.7	3.0	3.1	0.00014	2.3
56 2B	0.12	0.16	Δ/Y	230/400	2860	0.64/0.37	0.40	0.72	68.0	5.0	3.7	3.1	0.00015	2.8
56 2C	0.18	0.25	Δ/Y	230/400	2840	0.86/0.50	0.60	0.76	70.0	5.0	3.7	3.1	0.00016	3.2
63 2A	0.18	0.25	Δ/Y	230/400	2800	1.12/0.65	0.61	0.65	65.1	4.6	2.8	2.8	0.00014	3.4
63 2B	0.25	0.34	Δ/Y	230/400	2800	1.26/0.73	0.85	0.75	68.7	4.2	2.2	3.5	0.00017	4.0
63 2C	0.37	0.50	Δ/Y	230/400	2790	1.99/1.15	1.26	0.70	68.3	4.0	2.0	3.0	0.00018	4.5
71 2A	0.37	0.50	Δ/Y	230/400	2815	1.73/1.00	1.26	0.72	73.2	4.0	2.5	2.6	0.00033	4.9
71 2B	0.55	0.75	Δ/Y	230/400	2780	2.25/1.30	1.90	0.82	76.8	4.5	2.4	2.5	0.00042	6.0
71 2C	0.75	1.0	Δ/Y	230/400	2810	3.63/2.10	2.60	0.70	70.5	4.5	2.7	2.8	0.00054	6.4
80 2A	0.75	1.0	Δ/Y	230/400	2860	3.72/2.15	2.51	0.75	72.6	4.8	3.2	3.0	0.00062	7.5
80 2B	1.1	1.5	Δ/Y	230/400	2856	4.85/2.80	3.70	0.75	76.3	5.0	2.5	3.2	0.00078	8.6
80 2C	1.5	2.0	Δ/Y	230/400	2805	6.06/3.50	5.10	0.80	78.5	4.3	2.0	2.7	0.00085	9.9

Figure 5.2: Miksan Motor Catalogue

6 Alternative Design

6.1 Possible Alternative Solutions

In chapter 4 it has been shown how the second follower generates vibrations which are propagated along the rest of the system, resulting in a worsening of the dynamic behaviour of the mechanism. These vibrations are generated especially when the roller changes contact profile and hits the upper or bottom part of the second cam. The introduction of a torsional spring enhanced the behaviour of the system but vibrations are still present since the second roller is still changing contact profile. Possible solutions to this problem might be:

1. Changing the motion laws in order to avoid high jerks when the acceleration changes sign. Indeed, when the acceleration changes sign the roller changes contact profile and if the jerk at that instant is too high, the contact profile change is abrupt resulting in undesired vibrations.
2. Using a torsional spring able to keep the second roller always in contact to the lower part of the second cam. In this way changes in contact profile between second cam and roller are avoided, vibrations are reduced and only the lower profile of the second cam can be cut on a plate. The drawback is surely the use of a more expensive torsional spring.

In this chapter the results obtained from the dynamic analysis adopting the second solution are shown. The Adams Model is kept the same, only the torsional spring is changed and the upper profile of the second cam is not used.

6.2 Dynamic Analysis using Alternative Design

The torsional spring is again taken from the catalogue shown in figure 4.10. The spring chosen is the number $095P04$ having $k_T = 10.76 Nmm/^\circ$ and $P = 968.5 Nmm$.

6.2.1 Motion Law Comparison

Motion Law results are reported in figures 6.1 and 6.2. Regarding the first motion law, the acceleration peak at the beginning of the fall phase is disappeared due to the fact that the second roller does not hit anymore the upper profile of the second cam; while regarding the second motion law, the oscillations have almost totally disappeared due to the fact that the contact between roller and second cam is never changed.

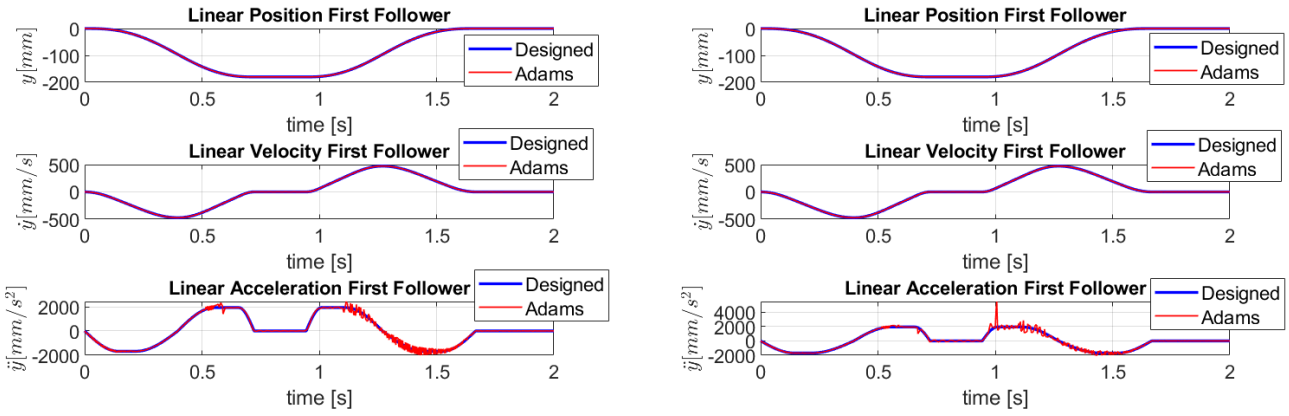

Figure 6.1: Comparison First Motion Law: left alternative design, right previous design

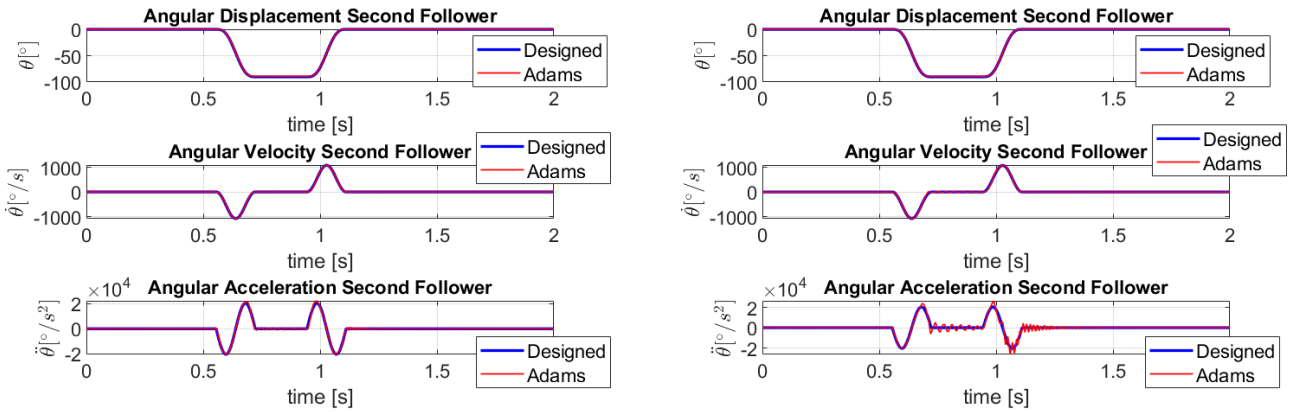

Figure 6.2: Comparison Second Motion Law: left alternative design, right previous design

6.2.2 Contact Forces Comparison

Contact forces comparisons are reported in figures 6.3 and 6.4. The oscillations in the contact forces are reduced both for first and second cam and the maximum force achieved is almost the same, meaning that the contact pressure check is still verified. Moreover, the peaks of the first cam internal contact have disappeared, meaning that the internal profile of the first cam works only during the dwell phase of the second motion law; this is due to the fact that only the lower profile of the second cam is in contact during operation.

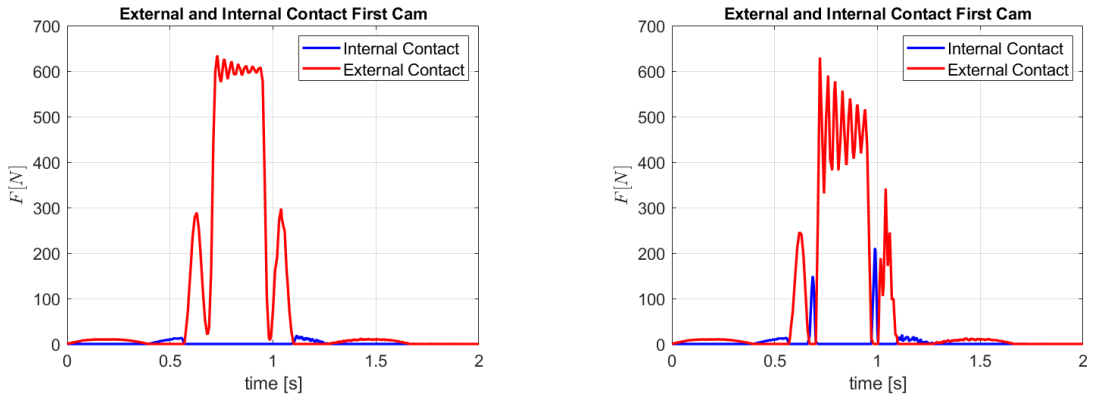

Figure 6.3: Comparison Contact Force First Cam: left alternative design, right previous design

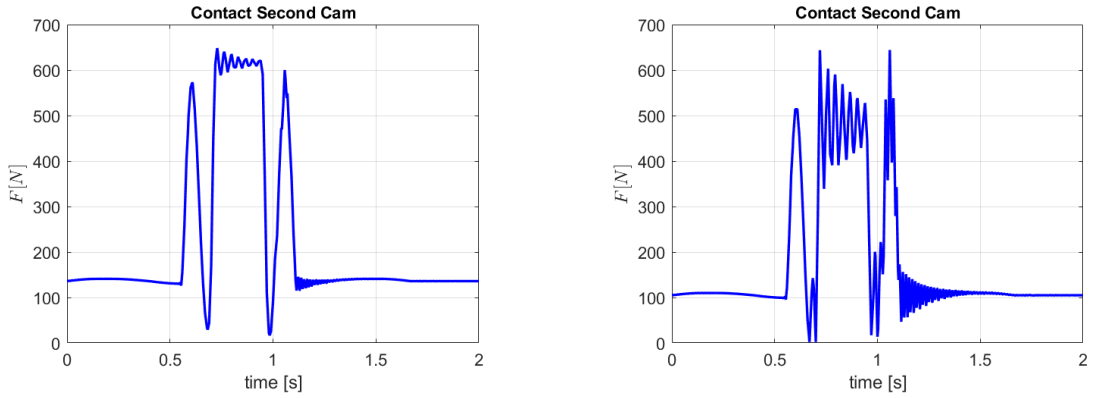

Figure 6.4: Comparison Contact Force Second Cam: left alternative design, right previous design

6.2.3 Slippage Check

Results for the slippage check are reported in figures 6.5, 6.6 and 6.7. It can be concluded that the rollers do not slip using this new design.

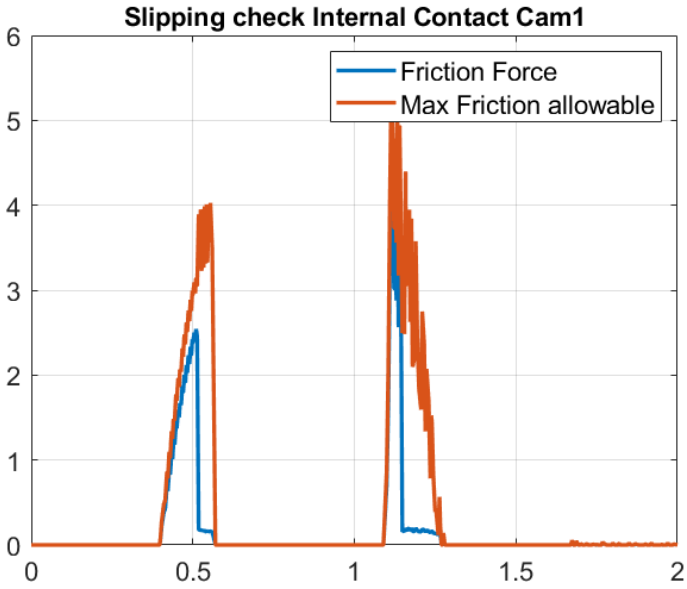

Figure 6.5: Slipping Check Internal Contact First Cam Alternative Design

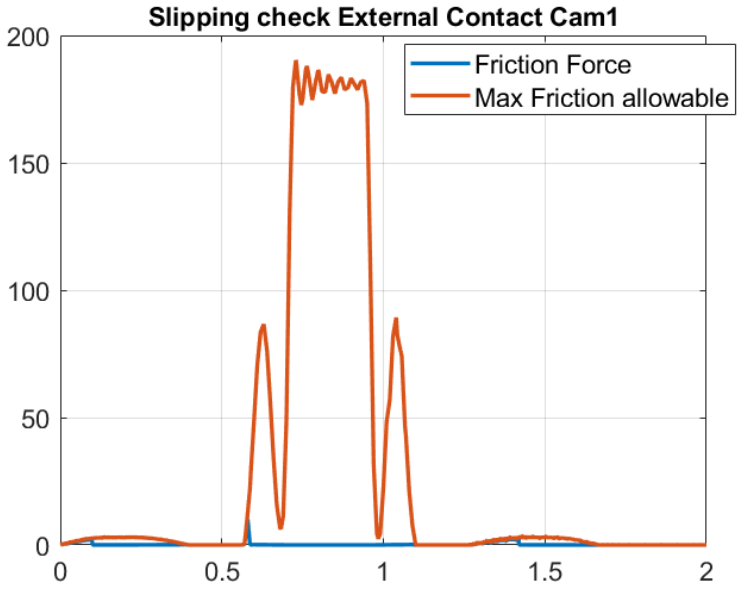

Figure 6.6: Slipping Check External Contact First Cam Alternative Design

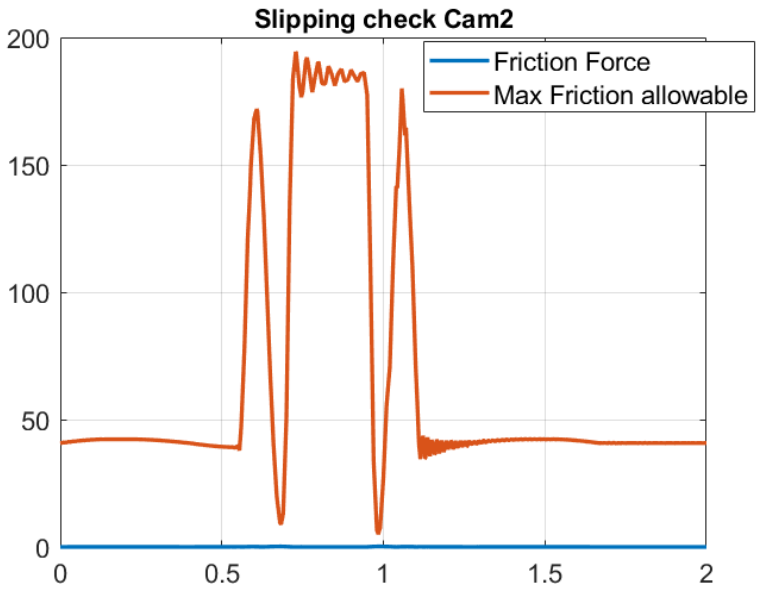

Figure 6.7: Slipping Check Contact Second Cam Alternative Design

6.2.4 Motor Torque Comparison

Motor torques required for alternative design and previous design are compared in figure 6.8. The alternative design has a lower maximum peak due to the fact that the second roller does not hit anymore the upper part of the second cam. Apart from that, the motor choice done previously is valid also for the alternative design since the maximum torque of the load was already very close to the maximum torque provided by the motor. Table 6.1 reports the new load characteristic parameters.

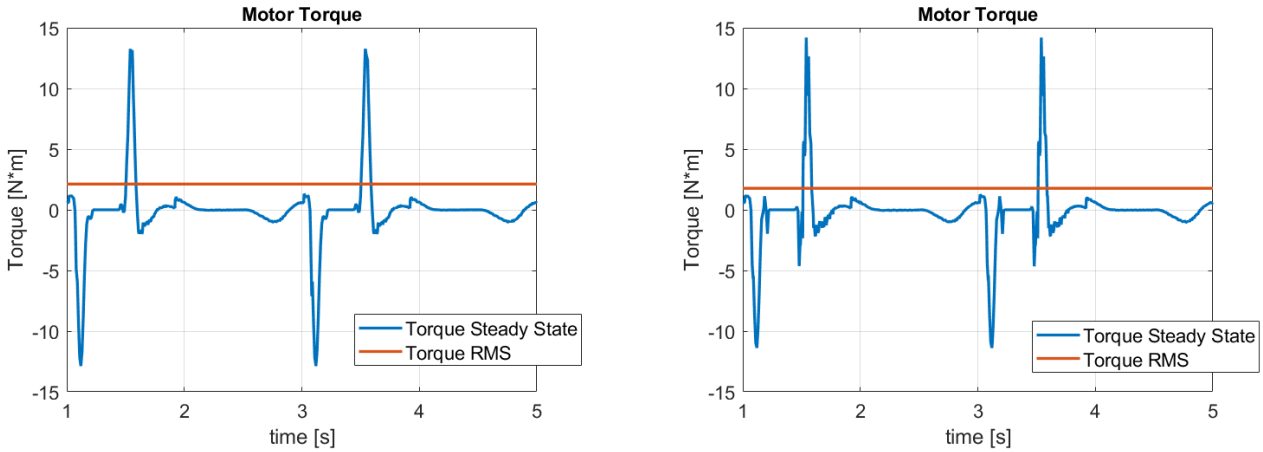

Figure 6.8: Comparison Motor Torque: left alternative design, right previous design

$T_{max}[Nm]$	$T_{RMS}[Nm]$	$\omega[rad/s]$
13.27	2.12	3.14

Table 6.1: Load parameters using Alternative Design

Bibliography

[1] Magnani, P. L. and Ruggieri, G. (1986). *Meccanismi per macchine automatiche*. Utet.